ANL-IFR-77

Simulant Material Pour Stream Breakup Tests and Model Implications

by J. D. Gabor, B. W. Spencer, and J. C. Cassulo

Argonne National Laboratory, Argonne, Illinois 60439
operated by The University of Chicago
for the United States Department of Energy under Contract W-31-109-Eng-38

SIMULANT MATERIAL POUR STREAM BREAKUP TEST AND MODEL IMPLICATIONS

by

J. D. Gabor, B. W. Spencer, and J. C. Cassulo

Reactor Analysis and Safety Division
Argonne National Laboratory
9700 South Cass Avenue
Argonne, Illinois 60439

IFR TECHNICAL MEMORANDUM NO. 77

~~Results reported in the IFR-TM series of memoranda frequently are preliminary and subject to revision. Consequently they should not be quoted or referenced without the author's permission.~~

~~APPLIED TECHNOLOGY~~

~~Any further distribution by any holder of this document or of the data therein to third parties representing foreign interests, foreign governments, foreign companies and foreign subsidiaries or foreign divisions of U. S. companies should be coordinated with the Deputy Assistant Secretary for Civilian Reactor Development, U. S. Department of Energy.~~

MASTER

~~Released for announcement in ATF. Distribution limited to participants in the LMFBR program. Others request from RSDT, DOE.~~

TABLE OF CONTENTS

Table of Contents (cont.)

LIST OF FIGURES

List of Figures (cont.)

LIST OF TABLES

SIMULANT MATERIAL POUR STREAM BREAKUP TESTS AND MODEL IMPLICATIONS

by

J. D. Gabor, B. W. Spencer, and J. C. Cassulo

ABSTRACT

The mechanisms of pour stream breakup and quench in a liquid coolant involved in reactor safety analysis are not readily predicted by existing correlations. Previous basic research has primarily been with small diameter jets (~ 1 mm) and with low density fluids (water, air, and organic liquids). However, pour streams of large diameter and high density (uranium oxides and alloys) are of interest to reactor safety analysis. Therefore an experimental study was conducted to examine the breakup and mixing behavior of initially coherent streams of high-density molten metals flowing into water. The breakup of ~ 20 mm pour streams was observed in a 152-mm ID glass column containing a 1.46-m pool of water. Molten Wood's metal was the pour stream material for the majority of the tests. Several experiments were also conducted with molten tin.

The test parameters included melt superheat, water subcooling, entrance velocity, and cover gas (air or steam). Single-phase convective heat transfer, nucleate boiling, and conditions conducive to film boiling were involved. The breakup length was characterized by the change in leading edge penetration rate in the water. In tests without net steam generation, the stream breakup length to initial stream diameter ratio measured 20 to 25 which is in reasonable agreement with the Taylor model; in tests with net steam generation (water at 100C), greater breakup length ratios of about 40 to 50 were obtained. The data for tests with steam generation agreed better with the Epstein and Fauske model when the density of steam was used for the ambient fluid.

Cover gas entrainment by the leading edge which dominated the initial penetration stage was reduced for the trailing pour stream column. The characteristics of the particles produced from the pour stream breakup were dependent on the test conditions. Flake-like particulate material was formed by freezing of the pour stream surface and separation from the flowing molten core. Filaments and globules resulted from surface tension forces. High-velocity pour streams resulted in finer fragmentation, whereas increasing melt temperature had little effect on the overall size distribution. The size of the mixing zone taken

to include metal fragments, vapor, entrained air, and the pour stream core was found to increase with increasing pour stream and water temperatures causing increased steam generation, except for the case when film boiling occurred resulting in a vapor envelope around the pour stream and therefore reducing heat transfer to generate steam.

I. INTRODUCTION

An understanding of the mechanisms of pour stream breakup and quench in a liquid coolant is required in analyses of reactor accident scenarios involving liquifaction of core materials and their downward migration into coolant in the vessel lower head region. If the molten core materials are quenched, a bed of solid particles is formed, and analysis would then assess the coolability of this bed. On the other hand, if the pour stream has not solidified as it passes through coolant, jet impingement heat transfer and attack by a melt layer must be considered. The purpose of this investigation was to visualize processes important to the jet breakup, quench, and solidification under a broad range of conditions to evaluate models for possible reactor-scale application.

Previous basic research[1-4] has primarily been with small diameter jets (in the order of 1 mm) and with low density fluids (water, air, and organic liquids). Reactor safety analysis is concerned with large diameter pour streams (> 20 mm) of high density materials (uranium oxides and alloys) in coolant.[5] In addition, consideration must be given to the effect of phase change of both the pour stream material (freezing) and the reactor coolant (boiling) on the breakup of the stream. However, previous investigations have contributed significantly to the understanding of the mechanisms of jet breakup and provide considerable information useful to safety assessments. These are discussed in the following.

A. Summary Review of Previous Work on Liquid-Jet Breakup

It has been observed that liquid jets, except in the case of atomization, maintain a continuous liquid core until an instability develops. This instability usually rapidly propagates until a discontinuity in the jet or breakup occurs. Instability depends on several parameters. For a given nozzle size and fluid, the breakup length is a function of jet velocity. Four regimes of breakup applicable to small diameter jets of low density fluids in gaseous atmospheres have been designated[4] and are sketched on Fig. 1.

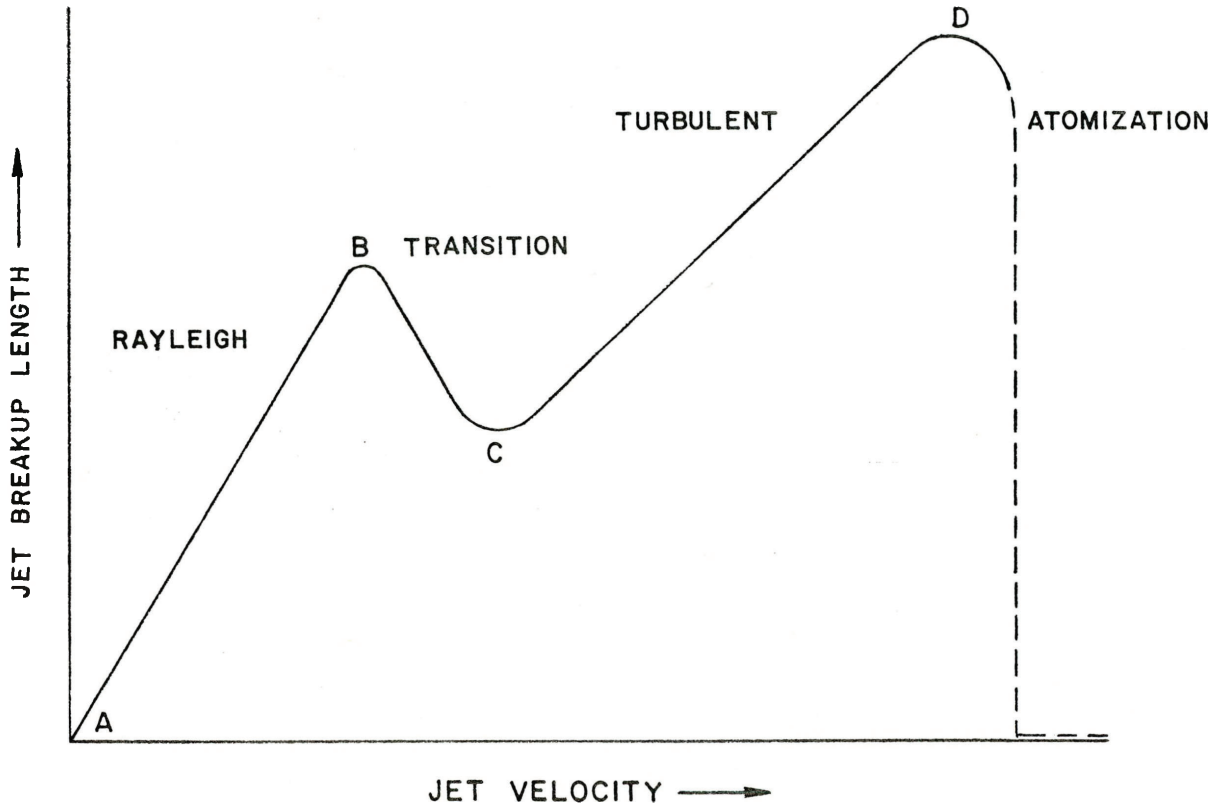

Figure 1. Jet Breakup Regimes[4]

B. Rayleigh Regime

The Rayleigh regime is the initial region of the curve on Fig. 1 in which the breakup length is a linear function of jet velocity. In this region the jet undulates symmetrically to form a varicose wave which grows and eventually leads to jet breakup. Rayleigh[6] modeled this regime with an inviscid fluid jet destabilized by surface tension and determined that the maximum instability occurred at a wave length

$$\lambda_{max} = 9.02 r_{ji} \tag{1}$$

As a result, during the time interval

$$t = 8.46 \sqrt{\frac{\rho_j r_{ji}^3}{\sigma_b}} \tag{2}$$

the amplitude of a disturbance increases e times, where r_{ji} is the jet radius, ρ_j is the jet density, and σ is the jet surface tension. Levich[7] then related the length of the jet at breakup, L, to initial jet velocity, u_o, by

$$L \approx u_o t = 8.46 u_o \sqrt{\frac{\rho_j r_{ji}^3}{\sigma}} \tag{3}$$

The resultant drops are approximately λ_{max} in diameter.

Weber[8] took into account the viscosity of the jet fluid undergoing symmetrical disturbances impressed on the jet flow. By neglecting higher order terms in the series expansion, Weber obtained

$$L = 12 \left[We^{0.5} + \frac{3We}{Re} \right] D_{ji} \tag{4}$$

where

D_{ji} is the jet diameter before breakup,

$$We = \frac{\rho_j U_j^2 D_{ji}}{\sigma}, \text{ and}$$

$$Re = \frac{D_{ji} U_j \rho_j}{\mu_j}.$$

The above models for this regime neglect the influence of the atmosphere.

Published experiments[1] indicate that the ambient Weber number defined as

$$We_a = \frac{\rho_a U_j^2 D_{ji}}{\sigma}$$

is less than 1.0 in this regime.

C. Transition Regime

In this region the inertial effects of the surrounding medium and jet turbulence become important. As is the case of transition regions, there is some uncertainty in defining it. Ranz[9] proposed that conditions for this regime required:

$$We_a > 0.4$$

Sterling and Sleicher[10] gave

$$We_a > 1.2$$

as a criterion for the transition regime.

Jet breakup occurs when a disturbance attains a wave length in the order of the jet diameter in the same manner as in the Rayleigh regime. The resultant drop diameter is about the same as the jet diameter.

D. Turbulent Regime

This regime, which is associated with wide data scatter, is indicated by CD on Fig. 1. Reitz[4] has described the breakup in this region as droplets

being stripped from the jet surface after a finite undisturbed length downstream. In this regime the ambient Weber number is generally stated in the literature as being greater than unity. Taylor[11] analyzed the generation of ripples by wind blowing over a viscous fluid. The wind was assumed to exert normal pressure on the surface but no tangential (frictional) stress on the free surface. This analysis was extended to the dispersion of larger diameter (20 mm) liquid-metal jets in water.[12] The length of the jet before breakup (system 1) was determined by comparison with existing data for jets and fluid atmospheres with different densities (system 2). The resulting equation is:

$$L_2 = L_1 \left(\frac{\rho_j}{\rho_f}\right)_2^{1/2} \Bigg/ \left(\frac{\rho_j}{\rho_f}\right)_1^{1/2} \tag{5}$$

Taylor used as a basis a breakup length of 150 jet diameters for a water jet in air and five jet diameters for a water jet in water. He, therefore, determined in the semi-empirical manner a jet breakup length of 14 to 15 jet diameters for a liquid metal in water.

Baron[13] obtained

$$L = 1.7\ (We)^{0.5} \left(Re \times 10^{-4}\right)^{-6.25} D_{ji} \tag{6}$$

for the turbulent regime.

E. Atomization

In this regime (DE in Fig. 1) the coherent length of the jet is essentially zero. This regime has been observed for small jet diameters (< 1 mm) and high velocity (> 100 m/s). The jet breaks up into a conically shaped spray of fine droplets at the nozzle. Littaye[14] derived a criterion of

$$We_a = 40.3$$

for the onset of atomization. Nozzle design is very important in this region.

Figure 1 should not be regarded as completely defining the phenomena of jet breakup. It was derived from experiments with small diameter jets (~ 1 mm) of light liquids (water and organics) primarily in a gaseous atmosphere. Data for liquid metal jets such as mercury and molten steel in air indicate departure from the Rayleigh regime at Weber numbers considerably less than unity.[1,15] In addition the regime which is termed turbulent does not necessarily indicate turbulent jet flow. Turbulence most likely had not developed in the jet flow stream in experiments with short injector tubes or nozzles. Breakup by sinuous wave formation is not included in this simple regime description. Sinuous wave formation is prevalent with large diameter jets.

Models and correlations for various mechanisms of jet breakup have been developed beyond the basic description of breakup regimes on Fig. 1. Some of the significant contributions will now be discussed.

F. Epstein and Fauske

Epstein and Fauske[16] considered the breakup of a jet blanketed by the vapor of the liquid in which it is injected. They assumed a wave form for the jet, vapor, and liquid phases which resulted in six algebraic equations, each equivalent to zero, with six unknowns. They set the determinant equal to zero to solve for the growth constant which does not solve for the unknowns. For a thick vapor blanket (essentially infinitely thick) following the method outlined by Levich,[7] they obtained:

$$L = \frac{\sqrt{3}}{2}\left(1 + \frac{\rho_v}{\rho_j}\right)\left(\frac{\rho_j}{\rho_v}\right)^{1/2} D_{ji} , \tag{7}$$

For a very thin vapor blanket with thickness essentially equivalent to zero,

$$L = \frac{\sqrt{3}}{2}\left(1 + \frac{\rho_\ell}{\rho_j}\right)\left(\frac{\rho_j}{\rho_v}\right)^{1/2} D_{ji} , \tag{8}$$

where subscripts v and ℓ refer to the vapor and liquid phases. It is noted that the final derivations do not include surface tension which was employed in the initial pressure condition equations.

G. Levich

Levich[7] discussed breakup lengths for jets having various characteristics. For jets with sinuous disturbances and low viscosity, μ_j, Levich gives the jet breakup length as

$$L \approx 5 \frac{u_o r_{ji} \mu_j}{\nu} \tag{9}$$

Levich also reports breakup lengths for high-velocity jets which atomize for short wave disturbances

$$L \approx r_{ji}(\rho_j/\rho_g) \tag{10}$$

Eq. 10 also applies to the case of long waves and low velocity. For long waves and a highly viscous fluid

$$L \approx \frac{\mu_{ji}}{\rho_g \mu_g} \tag{11}$$

All of the above lengths are for liquid breakup in gas and are so denoted by a g in the subscripts.

H. Grant and Middleman

Grant and Middleman[17] found that data for water and water solutions of glycerine, ethylene glycol, and ethanol in the Rayleigh regime were better correlated by

$$L/D_{ji} = 19.5 \left(We^{1/2} + 3 \frac{We}{Re} \right)^{0.85} \tag{12}$$

Their correlation for a turbulent jet is

$$L/D_{jj} = 8.51\ We^{0.32} \tag{13}$$

This can be compared with Phinney's[18] correlation

$$L/D_{jj} = 55 + 1.085\sqrt{We} \tag{14}$$

I. Hartel

Hartel[19] developed a linear model for the breakup length of liquid jets in a liquid continuum. Both liquids are characterized by low viscosity. The model is based on instability of varicose wave motion for vertical axisymmetric flow of the fluid jet. A computer program derived from this model calculated the jet breakup length as a function of jet diameter, velocity, density, viscosity, velocity profile, flow direction, and interfacial tension.

The model agreed quite well with data for toluene and methylisobutyl ketone jets ranging from 4 to 10 mm in diameter.[20] However, there was significant disagreement with Wood's metal data. Hartel predicted from his theory that the breakup lengths for 10-mm jets of uranium oxide in sodium and Wood's metal in water are the same.

In assessments of reactor accident scenarios, consideration must be given to phase change of both the jet fluid and the fluid environment. The jet fluid will be cooling down and most likely undergoing freezing whereas the coolant under certain conditions could be undergoing vaporization. Coolant vaporization has been postulated not only to change the ambient media but also during nucleate boiling to transfer momentum to the jet and contribute to its breakup, in contrast to the effect of the vapor envelope. These additional phenomena further complicate the mechanisms for jet breakup. Therefore, a series of experiments were conducted with simulant materials--low melting point metals and water--in a transparent apparatus on a scale of interest to safety analysis.

II. EXPERIMENTAL

A. Apparatus

The pour stream breakup tests were conducted in a transparent apparatus shown in Fig. 2. The breakup was observed in a glass column constructed of 6-in. (152.4-mm) ID Pyrex pipe joined together by flanges. The water contained within in the column was heated by nichrome strip heaters attached to the external wall of the Pyrex pipe. The melt furnace/injector was mounted on top of the Pyrex column. Two furnaces were used in these tests. The furnace used in the majority of the experiments had a capacity for 2.0 kg of metal. The one shown in Fig. 2 had a capacity of more than 12 kg of metal. The furnaces were wrapped with trace heaters and thermal insulation. Argon was used as the cover gas. The diaphragm cutter for the smaller furnace was a section of a tube with a 28.6-mm OD and a 27.0-mm ID. The cutter edge was at a slight angle which folded the cut portion of the diaphragm back along the inner surface of the nozzle during injection. The effective flow area of the melt was considered to be the inside area of the cutter. Injection was initiated by a solenoid valve pressurizing an air cylinder driving a cutter through a 0.05 mm stainless steel diaphragm. A 25.4-mm diameter nozzle or drop tube 206-mm in length was attached below the diaphragm. All of the tests were conducted with the system vented through a trap seal to the atmosphere. This prevented the buildup of high steam pressure in the apparatus during tests.

The instrumentation for indicating conditions in the mixing vessel consisted of thermocouples and pressure transducers. The locations of the thermocouples (indicated by TC's) and the pressure transducers (PTS's) are shown on Fig. 2. Three thermocouples were located at 45, 90, and 140 mm from the bottom of the larger melt furnace. Two thermocouples at 20 and 40 mm from the bottom of the small melt furnace were used for determining the metal melt temperature. The thermocouples were chromel-alumel enclosed in a 1/8-in. (3.2 mm) diameter grounded stainless steel sheath. Strain gauge transducers (Dynisco and Statham in the 0 to 100 psi range) were located in the freeboard space above the water level and at 0.22 and 0.85 m above the base of the column in the water as well as on the melt furnace.

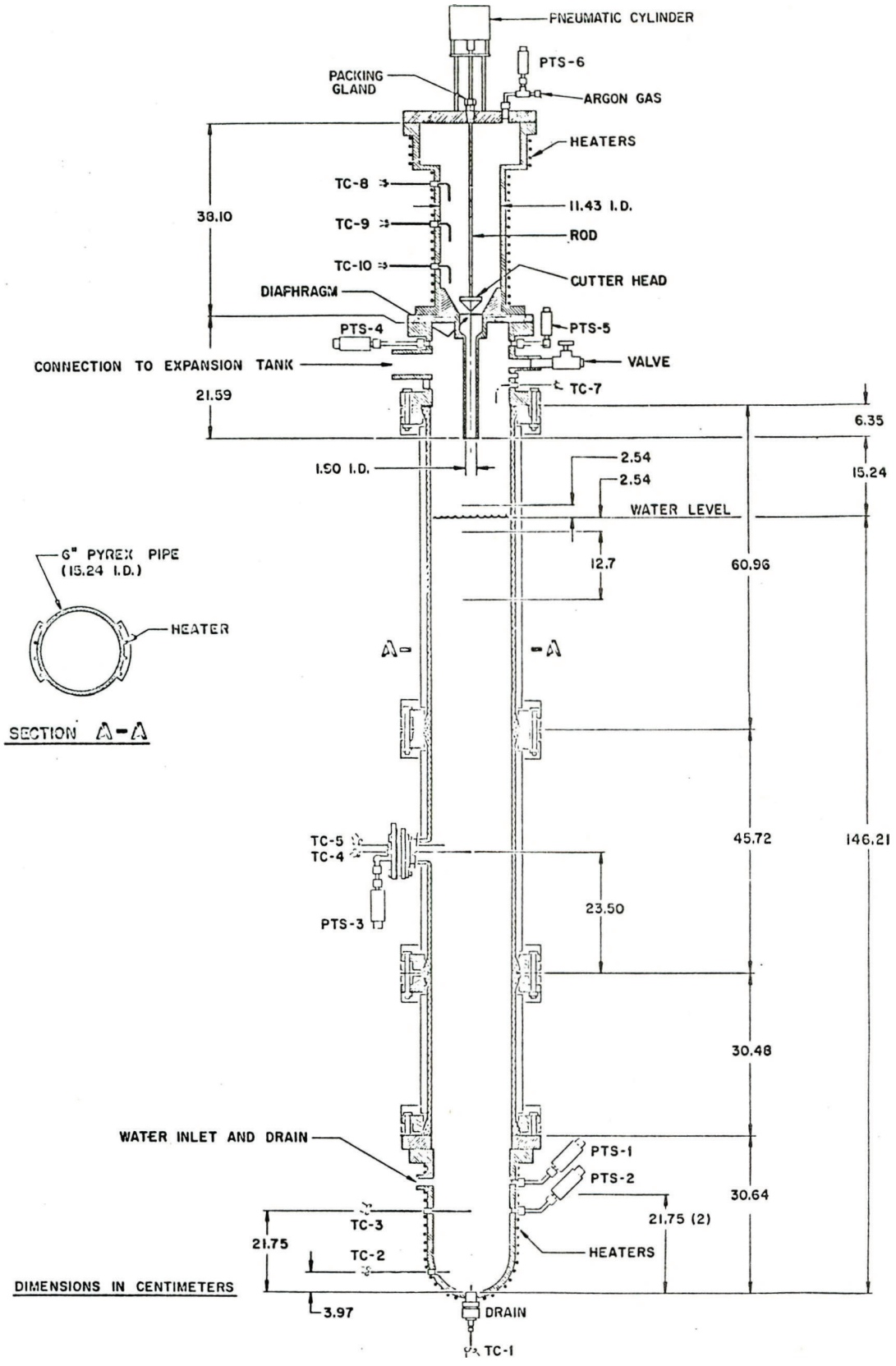

Figure 2. Apparatus for Pour Stream Breakup Experiments

The thermocouples were monitored by a Doric Trendicator 400A during the heatup phase. A Honeywell 101 magnetic tape unit and a Honeywell 1858 visicorder were used to record thermocouple and pressure transducer data. Weathermeasure and Shinko controllers were used to regulate the melt furnace and Pyrex column heaters. Five HYCAM cameras (Red Lake Laboratories) operating at 500 fps were used to obtain motion pictures of the jet breakup and mixing. Four cameras were focused for localized views which sufficiently overlapped so as to cover the entire depth of water. The remaining camera photographed the entire column length.

In some experiments it was desired to eliminate air entrainment by the jet. This was achieved by purging the freeboard space above the water pool with steam produced by a steam generator. The freeboard atmosphere was analyzed by trapping the outflow in a heated sample bomb with a pressure gauge and then quenching the bomb with cold water to condense the steam. The steam quality was then determined from the pressure change correcting for the vapor pressure of the condensed water at the temperature of the cooled bomb. Experiments were conducted with the steam concentration ranging from 90 to 98 volume %. In experiments with the water at saturation temperature, the steam was generated by the water pool.

B. Melt Materials

For these tests metal materials were used for the pour stream phase material which were convenient for experimentation in water and a glass container. The metals which were used were tin and Wood's metal (50 w/o Bi - 25 w/o Pb - 12.5 w/o Cd - 12.5 w/o Sn). The melting point of Wood's metal is 70C and therefore will not solidify in water at T_{sat}. Reference is made in this report to tests with Cerrotru alloy (Cerro Metal Products, Bellefonte, PA) and U - 5 w/o Zr alloy.[21,22] The Cerrotru alloy is a eutectic mixture (58% Bi - 42% Sn) and therefore the solidus and liquidus points are the same. The breakup of U - 5 w/o Zr alloy pour streams in sodium coolant was studied in a series of tests.[23] Physical properties of these materials are listed in Table I.

TABLE I. Heat Transfer Properties

Material	T_{mp},K	ρ_s,kg/m^3	ρ_ℓ,kg/m^3	μ_ℓ,Pa·s	λ,kJ/kg	C_{p_s},kJ/kg·K	C_{p_ℓ},kJ/kg·K	K_s,W/m·K	K_ℓ,W/m·K
Water	298.2	-	1000.5	0.894×10^{-3}	-	-	4.181×10^{3}	-	0.597
Water	373.2	-	9580	0.284×10^{-3}	2.257×10^{3}	-	4.215	-	0.680
Tin	505	7000	5613	2.62×10^{-3}	58.9	0.219	0.22	60.0	30.3
Wood's Metal	343.2	9200	9200	1.6×10^{-3}	46.51	0.15	0.172	13.31	12.64
Cerrotru	411.2	8672	8672	1.8×10^{-4}	46.5	0.175	0.184	17.6	-
U-5w/oZr	1450[a]	15900	-	-	60	0.170	-	52	-
U-5w/oZr	1524[b]	-	15.4	6.0×10^{-3}	60	-	0.210	-	33

[a]Solidus temperature

[b]Liquidus temperature

C. Test Parameters

A series of experiments designated JC (jet coolant) were conducted using molten Wood's metal and tin for the pour stream phase. Various parameters were selected to determine their effect on the pour stream breakup and the characteristics of the particles produced by the breakup. The parameters included melt superheat, water subcooling, entrance velocity, and cover gas (see Table II). Single-phase convective heat transfer, nucleate boiling, and conditions conducive to film boiling were involved.

These experiments required some developmental effort in order to achieve good continuous pour streams, desired conditions, and consistent operation of the instruments. As a result several tests were repeated in order to obtain a properly recorded test. Tests will be initially described in terms of observations.

D. Test Observations

1. Pour Stream Drop in Air

This test was conducted to determine the pour stream breakup length in gas by removing the water from the glass column to allow the pour stream to drop through air. This test was a point of reference for stream flow velocity and breakup behavior in a completely gaseous environment in comparison with pour stream behavior in a high voidage steam/water mixture. The Wood's metal was slightly pressurized above atmospheric (20 KPa) to give an initial velocity of 2.4 m/s. The pour stream maintained its integrity with no tendency for breakup during the entire length of the drop (1.31 m or $L/D_{jj} = 66$) (see Fig. 3). The leading edge tended to become spherical because of surface tension force (Fig. 3c) and the stream surface remained smooth. The stream diameter became smaller because of the stretching out effect of gravity acceleration. Several of the reported models predict a breakup length shorter than the length (1.31 m) observed in this test.[6,16] However, a calculation (Appendix D) based on the drag force on a spherically shaped leading edge compared to the surface tension force indicates a breakup length of 9.5 m.

TABLE II. Conditions for Jet-Coolant Test Series

Test	Charge, kg	Material	Melt Temp, °C	Cover Gas	Water Temp, °C	Charge Press, KPa	Fragment Bed Voidage	Comments
JC-1	1.992	WM	95	Air	22	0	0.710	
JC-2	1.995	WM	89	Air	23	0	0.648	Wood's metal not completely melted.
JC-3	1.999	WM	89	Air	24	517	0.507	Pressurized injection. Fine debris
JC-4	2.003	WM	213	Air	23	0	0.636	High melt temperature.
JC-5	2.010	WM	234	Air	21	517	0.630	Pressurized injection. High melt temperature.
JC-6	2.024	WM	86	Air	22	0	0.625	Vent line plugged. Thin pour.
JC-7	2.016	WM	210	Air	22	0	0.625	Vented. High melt temperature.
JC-8	2.054	WM	113	Air	24	0	0.654	Plug in vent line.
JC-9	2.044	WM	100	Air	23	21	0.715	Slight gas pressure improved vent.
JC-10	1.846	Tin	319	Air	22	21	-	Tin drop. Large irregular fragments.
JC-11	1.805	WM	109	Air	22	21	0.750	Full diameter pour.
JC-12	1.841	WM	104	Steam	99	21	-	Full diameter pour in saturated water.
JC-13	1.855	WM	318	Steam	100	21	-	High melt temperature and saturated water.
JC-14	1.763	Tin	303	Steam	100	21	-	Thready pour.
JC-15	1.561	Tin	307	Air	25	21	-	Smaller charge than 10. Vapor explosion.
JC-16	1.441	Tin	295	Steam	100	21	-	Repeat of 14. Thin but steady pour.
JC-17	1.992	WM	95	Air	25	21	0.734	Repeat of earlier runs.
JC-18	1.816	WM	123	Air	21	21	0.731	Repeat of earlier runs.
JC-19	1.934	WM	116	Steam	100	21	-	Repeat of earlier runs. Good injection.
JC-20	1.981	WM	105	Steam	25	21	0.647	Steam cover on low temperature water.
JC-21	1.998	WM	92	Steam	24	21	0.589	Steam cover not good.
JC-22	2.035	WM	90	Steam	25	21	0.580	Thready pour.
JC-23	1.974	WM	125	Air	-	-	-	Air drop.
JC-24	1.972	WM	445	Steam	100	21	-	High temperature melt in saturated water.
JC-25	2.030	WM	86	Steam	25	21	0.681	Problems with cameras.
JC-26	2.035	WM	89	Steam	20	21	0.671	Good pour at start.
JC-27	1.846	WM	86	Steam	25	21	0.574	Good pour at start.
JC-28	1.984	WM	101	Steam	23	21	0.676	Good pour.
JC-29	2.000	WM	127	Steam	101	21	-	Repeat of 19.
JC-30	2.037	WM	200	Air	19	21	0.695	Repeat of 7. Thready pour.
JC-31	1.975	WM	310	Steam	101	21	-	Repeat of 13.
JC-32	1.938	WM	223	Air	23	21	0.674	Repeat of 30.

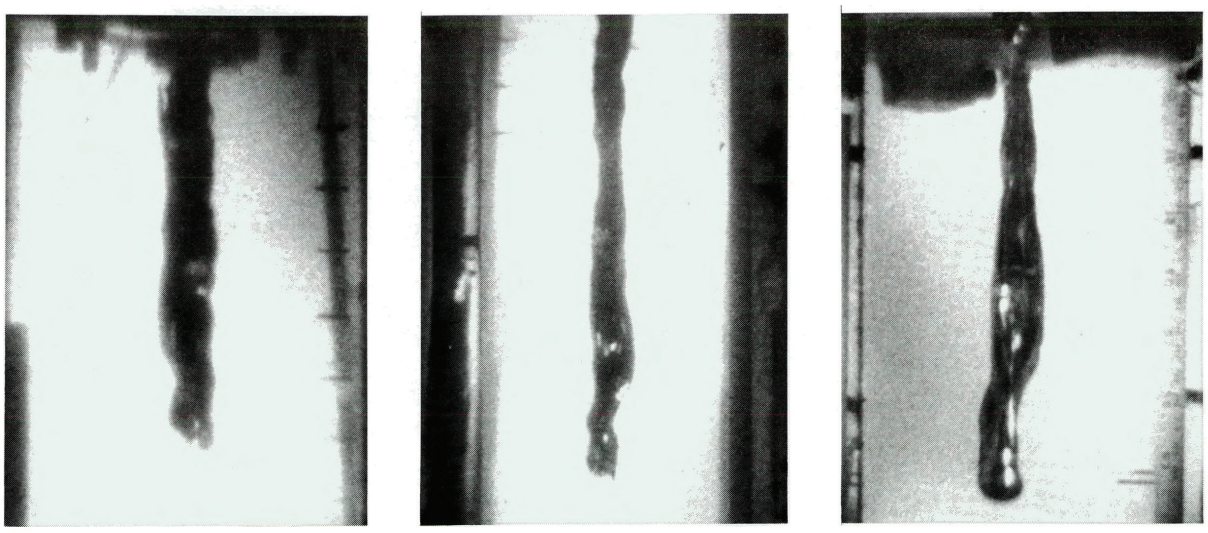

(a)

t = 0.056 s, L = 0.152 m (distance below nozzle)

(b)

t = 0.118 s, L = 0.340 m

(c)

t = 0.236 s, L = 0.812 m

Figure 3. Photographs of Jet Drop in Air (JC-23)

2. No Boiling

Tests were conducted with no water boiling and with boiling generated by the molten Wood's metal stream. The boiling can affect the breakup by transferring momentum to the pour stream in the case of nucleate boiling and by reducing the drag on the pour stream by enveloping it with vapor in the case of film boiling. Tests conducted with conditions so that water boiling did not occur reveal the single-phase water-environment breakup mechanisms.[21]

In JC-20 the water pool was at 25C and steam was injected into the freeboard above the water pool to displace the air. The steam atmosphere eliminated entrainment of noncondensable air as the pour stream penetrated into the top surface of the water. This can be seen from the photographs for the JC-20 drop in which the Wood's metal was initially at 105C (Fig. 4). The breakdown of the pour stream appears to occur by stripping off of undulations (Fig. 4d) in the form of what have been termed shearing puffs by Reynolds.[24]

The atmosphere above the water pool for JC-32 was air. As a result entrainment of the noncondensible air above the water pool was observed as the pour stream entered the water (see Fig. 5). The entrainment sac (Figs. 5c and 5d) collapsed about 0.12 s after pour stream entry into the water. Blunting of the leading edge to about twice its previous diameter on initial impact of the pour stream is shown on Fig. 5b. After this initial distortion of the pour stream, subsequent disturbances were on the surface of the pour stream (Figs. 5c and 5d).

It is seen that the breakup is related primarily to leading edge instability and to the trailing column instabilities, both causing disentrainment of material. In the latter case, the observed instability is not limited to the classical Kelvin-Helmholtz instability, although there is visual evidence for this in the photos, but also includes sinuous wave and pedal breakdown at reduced pour stream column diameter.

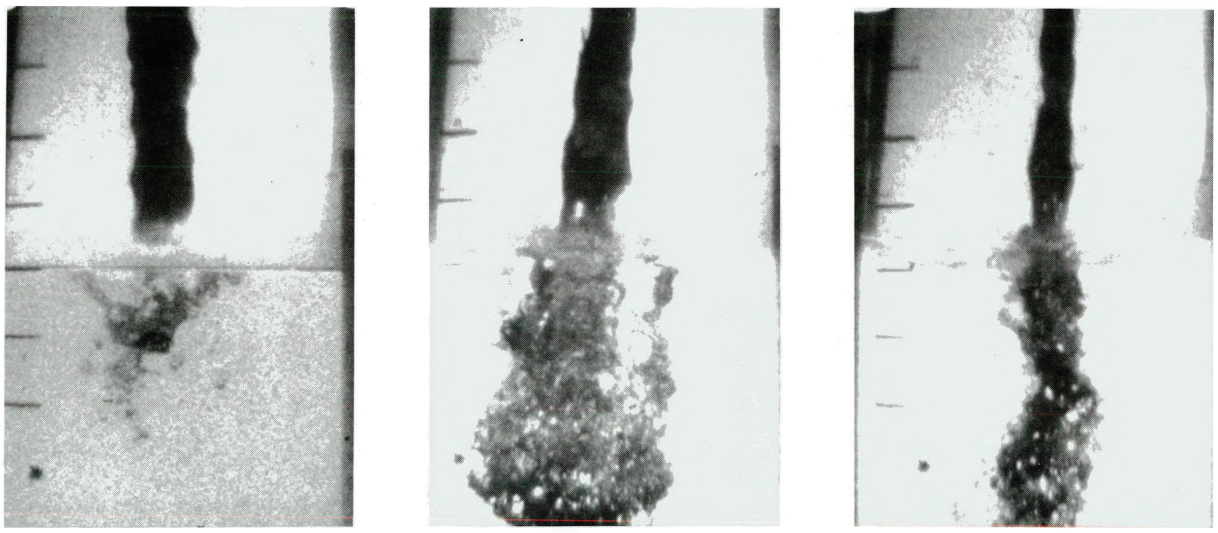

(a)

t = -0.002 s, L = -.009 m (above water level)

(b)

t = 0.044 s, L = 0.063 m

(c)

t = 0.148 s, L = 0.282 m

Figure 4. Injection with Steam Cover Gas (JC-20)

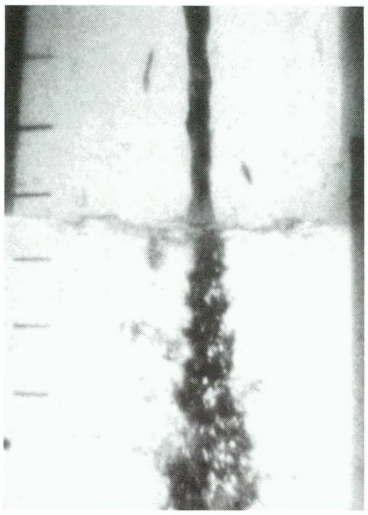

(d)

t = 0.258 s, L = 0.456 m

(e)

t = 0.118 s, L = 0.219 m

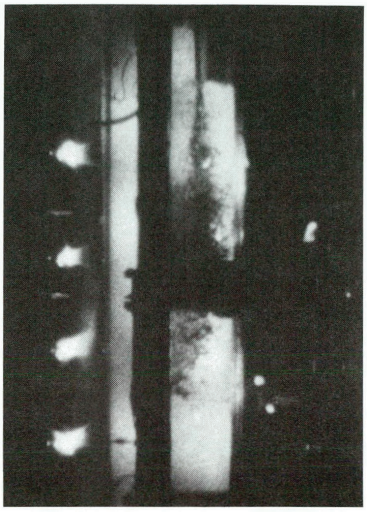

(f)

t = 0.346 s, L = 0.566 m

Figure 4 (cont). Injection with Steam Cover Gas (JC-20)

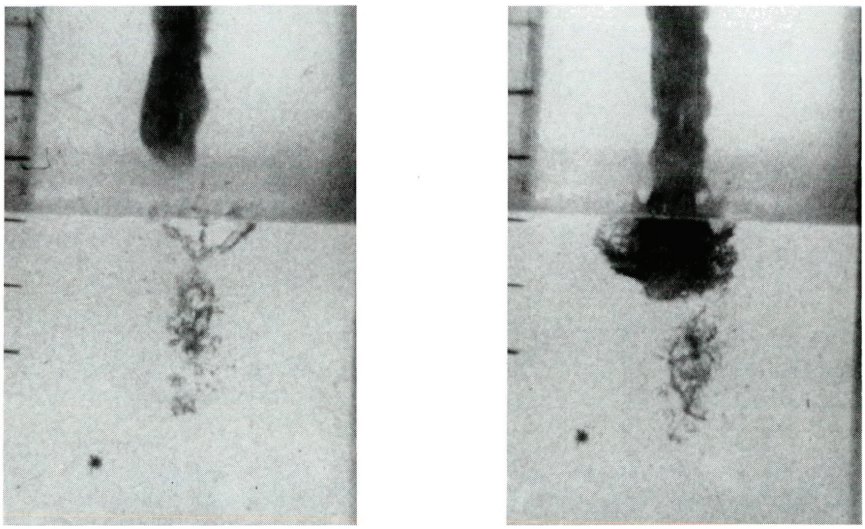

(a)

t = -0.008 s, L = -0.017 m

(b)

t = 0.018 s, L = 0.038 m

Figure 5. Injection with Air Cover Gas (JC-32)

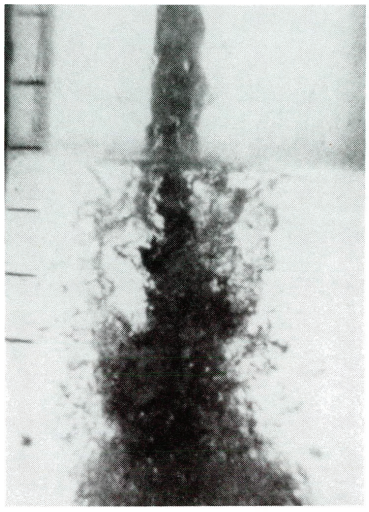

(c)

t = 0.058 s, L = 0.168 m

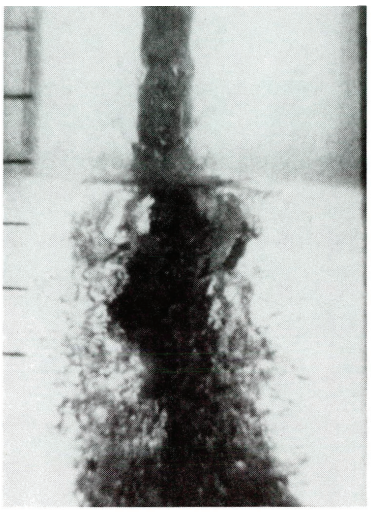

(d)

t = 0.070 s, L = 0.201 m

Figure 5 (cont). Injection with Air Cover Gas (JC-32)

3. Nucleate Boiling

Tests were conducted with Wood's metal and tin pour streams into water at its boiling temperature. The heat transferred from the pour streams to the water in these tests was translated into a phase change in the water (boiling). A sequence of photographs from JC-19 of the Wood's metal pour stream initially at 116C proceeding through the water is shown in Fig. 6. Nucleate boiling occurred at these conditions. Figure 6a shows the pour stream prior to entering the water. Preceding the main pour stream are a few drops of the melt. These drops were produced when the diaphragm was cut and the main stream formed. When these drops contacted the water, they initiated localized boiling. The vortex ball at the leading edge was approximately two times the initial pour stream diameter. Figure 6b shows the pour stream after it has penetrated 89 mm into the water. An entrainment sac is seen to envelop the pour stream as it enters the water. While steam was formed in the freeboard space by vaporization from the surface of the water pool, there was no prior purge of air by steam from the steam generation. The entrainment sac collapsed after 0.116 s. A blanket of steam is formed around the pour stream with very little mushrooming of the leading edge as in the cases with the water at room temperature where the leading edge impacted into the water surface (see Fig. 5b for JC-32). Figure 6d shows the leading edge of the pour stream 210 mm below the initial water level. Dispersion of fragments from the leading edge has begun and as a result vapor generation is increased near the leading edge compared to the region near the following flow stream. The leading edge is 335 mm below the initial water level in Fig. 6e. The mixing zone defined by particles and vapor bubbles has expanded to the walls of the container.

4. Film Boiling

The purpose of JC-24 was to observe the breakup of a pour stream with film boiling of the coolant phase at the stream surface. The Wood's metal melt was heated to a temperature of 445C which was the upper limit of the furnace, and the water was at saturation temperature (100C) A minimum temperature of 379C was determined for the pour stream-water interface temperature to exceed the homogeneous nucleation temperature of 305C for water (see

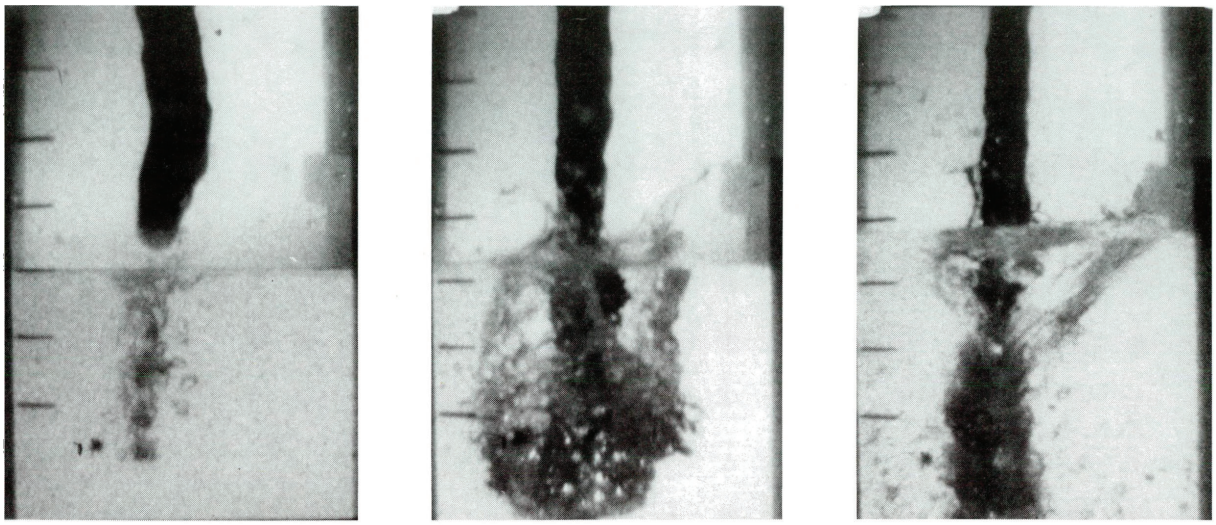

(a) t = -0.002 s, L = -0.007 m

(b) t = 0.036 s, L = 0.089 m

(c) t = 0.100 s, L = 0.241 m

Figure 6. Water at 100C and Wood's Metal Jet at 116C (JC-19)

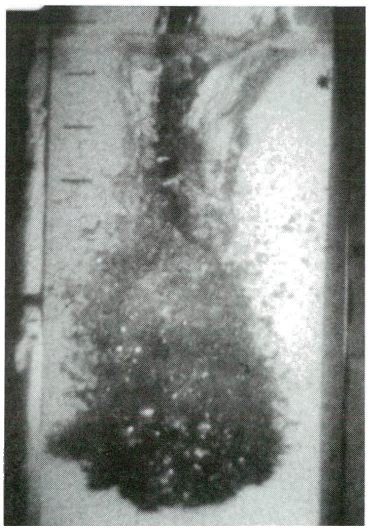

(d)

t = 0.086 s, L = 0.210 m

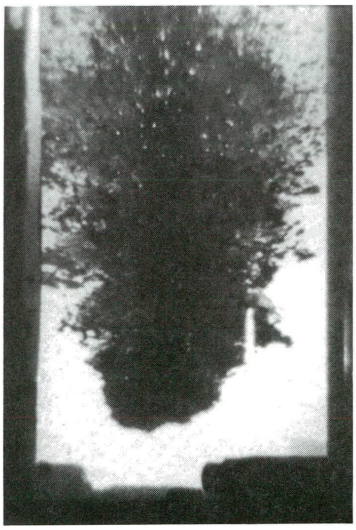

(e)

t = 0.136 s, L = 0.335 m

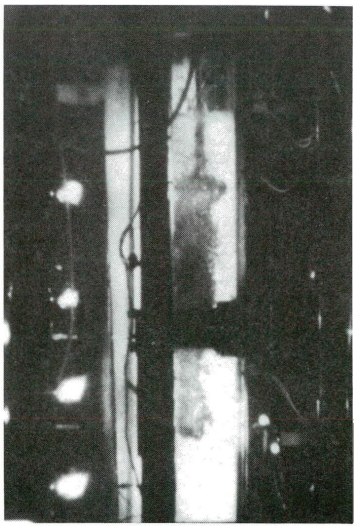

(f)

t = 0.234 s, L = 0.615 m

Figure 6 (cont). Water at 100C and Wood's Metal Jet at 116C (JC-19)

Appendix C). However, a minimum bulk temperature of 556 to 585C for the pour stream was calculated from Henry's Correlation (Appendix C) to be required for film boiling.

Figure 7 shows the pour stream of JC-24 as it progresses through the water. The pour stream prior to entering the water pool is shown in Fig. 7a. The marks on the glass column are 25.4 mm apart. Drops of melt which preceded the main body of the jet were formed when the diaphragm was cut. These drops fell into the water and generated some small localized boiling below the water level. Figure 7b shows the pour stream after the pour stream had penetrated about 23 mm below the interface. The leading edge of the pour stream is seen to be blanked by steam. Figure 7c shows the main body of the stream near the upper surface of the water after flow has developed. It is seen that the pour stream has maintained its integrity and that the vapor blanket is relatively thin indicating the insulating effect of the vapor. Figure 7d shows the upper portion of a large slug-like bubble which was formed. On Fig. 7e is the lower portion of the bubble generated by the leading edge fragments.

An overall view of the pour stream is shown in Fig. 7f. A large vapor region is shown in the center. The leading edge particles at this time had cooled sufficiently not to further generate boiling. The average void fraction defined as the vapor volume divided by the estimated volume of the mixing zone is approximately 0.25.

Unlike test JC-23 where the pour stream fell through air and no breakup occurred, breakup was observed in JC-24. It is concluded then that the pour stream was not completely blanketed by vapor so as to be prevented from liquid water contact in its traverse through the water column. Liquid water evidently contacted the melt stream because of inertia effects and apparently its temperature was insufficient to maintain film boiling as determined from Henry's correlation.

The effect on the water level by the increased boiling can be seen by the sequence of photographs of Fig. 7a, 7b, 7c, and 7d. Significant swelling resulted with the entire freeboard space eventually filled. Pool expansion is further discussed below (Section E.5).

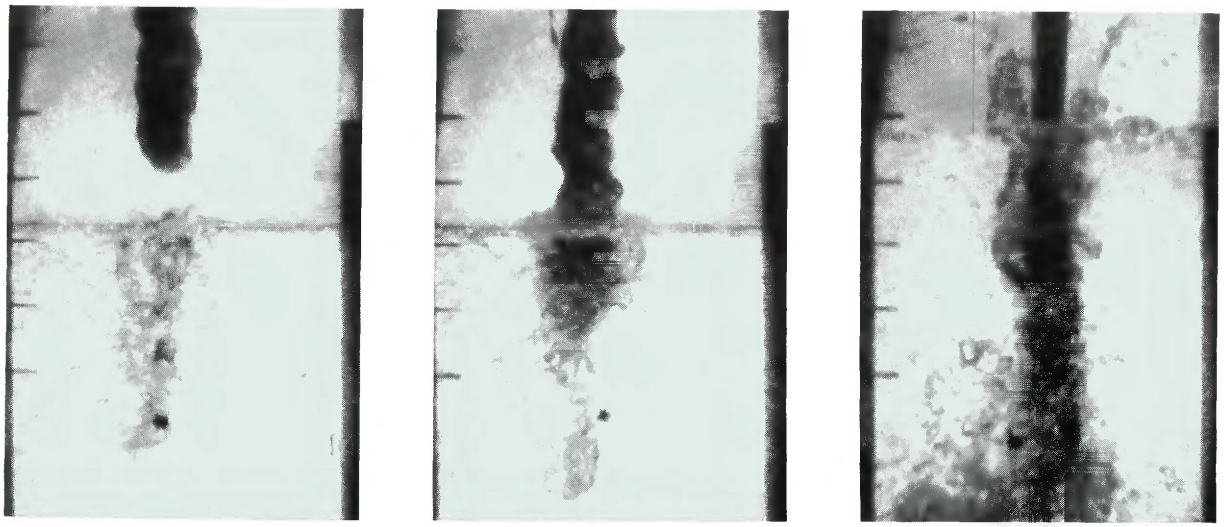

(a) t = -0.006 s, L = -0.019 m

(b) t = 0.012 s, L = 0.023 m

(c) t = 0.162 s, L = 0.296 m

Figure 7. Photographs of High-temperature Pour Stream in 100C Water (JC-24)

(d)

t = 0.392 s, L = 0.648 m

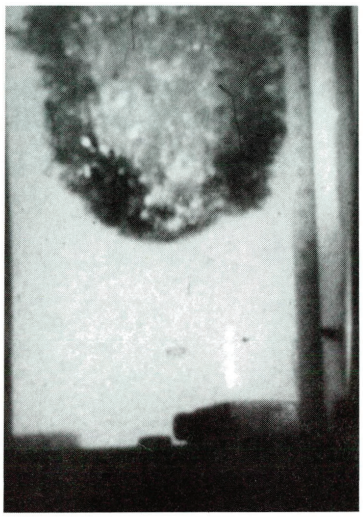

(e)

t = 0.154 s, L = 0.284 m

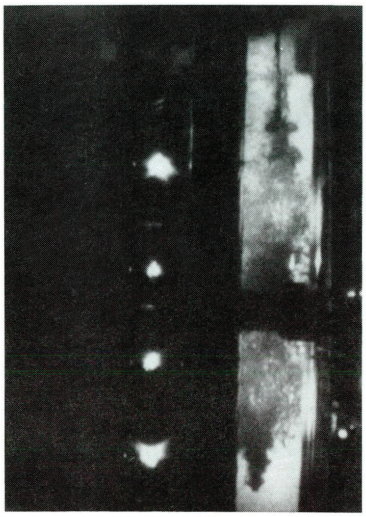

(f)

t = 0.452s, L = 0.725 m

Figure 7 (cont). Photographs of High-temperature Pour Stream in 100C Water (JC-24)

5. High Velocity Pour Streams

Tests were conducted with the injector pressurized to 517 KPa with argon gas resulting in an increase in the stream velocity to 6.0 m/s from about 2.6 m/s with 21 KPa pressure. The Wood's metal temperature was 89C in JC-3 and 234C for test JC-5. It appeared that accelerating the pour stream by increasing the pressure in the injector with argon resulted in two-phase flow. The stream diameter was larger than for the pour streams which were not pressurized (see Fig. 8). Figure 8b shows a lateral bulge in the pour stream above the water level caused by expansion of the entrained argon phase. Figures 8c and 8d continue the sequence of the pour stream as it penetrates downward. The mixing zone consisting of melt drops, particles, vapor, and argon gas (used to pressurize the melt furnace) almost immediately expands to the walls of the glass container. A jet of argon gas followed the melt pour stream causing the water pool to expand and overflow with entrained metal particles and gas.

While this technique of increasing gas pressure in the furnace/injector did increase the velocity of melt flow, it resulted in a two-phase stream behavior which was not comparable with the previous tests.

6. Tin Drops

These tests were conducted with tin as the melt material. Tin has a higher melting point (232C) than Wood's metal (73C) and will solidify in boiling water. Tin, however, has a propensity toward explosive behavior in water which is not an issue with sodium coolant in fast reactors.[22] This explosive nature is illustrated in test JC-15 with the water at 25C. Figure 9a shows the initial penetration by the pour stream into water. There is bubbling around it most likely because of a combination of entrained air and boiling. Figure 9b, 0.018 s later than Fig. 9a, shows the rapid increase in pour stream fragmentation and the size of the mixing zone resulting from an explosive interaction. Several other subsequent explosions were observed. The explosions were nonenergetic and did no damage to the Pyrex apparatus.

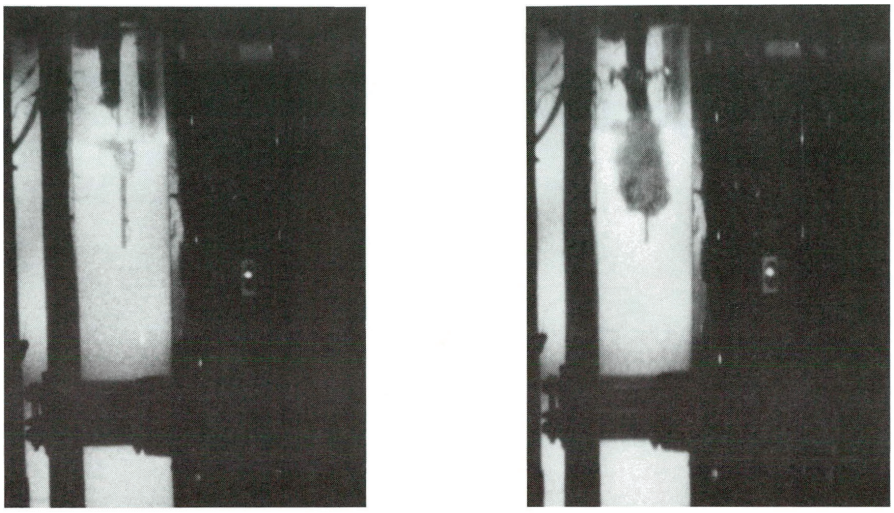

(a)

t = -0.006 s, L = -0.051 m

(b)

t = 0.024 s, L = 0.102 m

Figure 8. Pressurized Pour Stream Injection (JC-5)

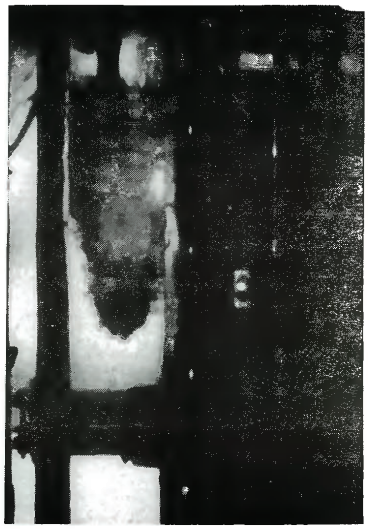

(c)

t = 0.066 s, L = 0.276 m

(d)

t = 0.142 s, L = 0.517 m

Figure 8 (cont). Pressurized Pour Stream Injection (JC-5)

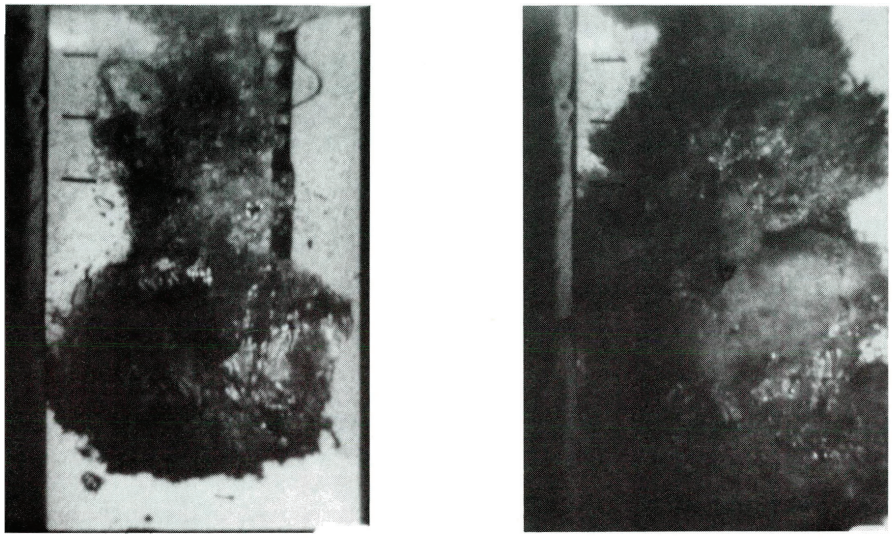

(a) (b)

t = 0.092 s, L = 0.174 m t = 0.110 s

Figure 9. Mild Explosion from Tin-Water Interaction (JC-15)

No explosions, however, were observed in test JC-16 with the water temperature at 100C. This is attributed to vapor blanketing at the tin surface which limited contact with the water as can be seen from the sequence of photographs on Fig. 10.

E. Discussion

1. Particle Formation

The characteristics of the particles produced by the pour stream breakup were dependent on the test conditions. No solid particles of Wood's metal were formed in tests with the water temperature exceeding the freezing point (70C) of the Wood's metal. Globules were formed by surface tension force acting to reduce the surface area. Filaments (thread-like particles) also resulted from surface tension forces acting on molten particulate material with freezing occurring before globules could be formed. Sheet- or flake-like particles were formed by freezing of the surface of the pour stream and separation from the flowing molten core. These are illustrated by the particles from JC-1 (photographs on Fig. 11). About 76 w/o of the particles were in the range of 2.4 to 9.5 mm (size distribution is tabulated in Table III).

In test JC-4 the melt temperature was increased to 213C compared to 95C for JC-1. This resulted in more time for globule formation before the molten jet drops froze (see Fig. 12). The overall size distributions for the two tests (see Table III) were about the same with 76 w/o particles in the 2.4 to 9.5 mm range. This indicates that there is essentially no further breakdown of the drops after pour stream breakup.

The high-velocity pour stream of JC-5 caused finer breakup of the pour stream with 42 w/o of the material in the 2.4 to 9.5 mm range. Typical portions of the particulate are shown on Fig. 13.

Figure 14 shows the frozen particles from a tin drop (JC-10). The particles were larger than for the Wood's metal experiments. This is attributed to the higher thermal conductivity of the tin (see Table I) in that freezing occurred before extensive hydrodynamic breakup of the pour stream

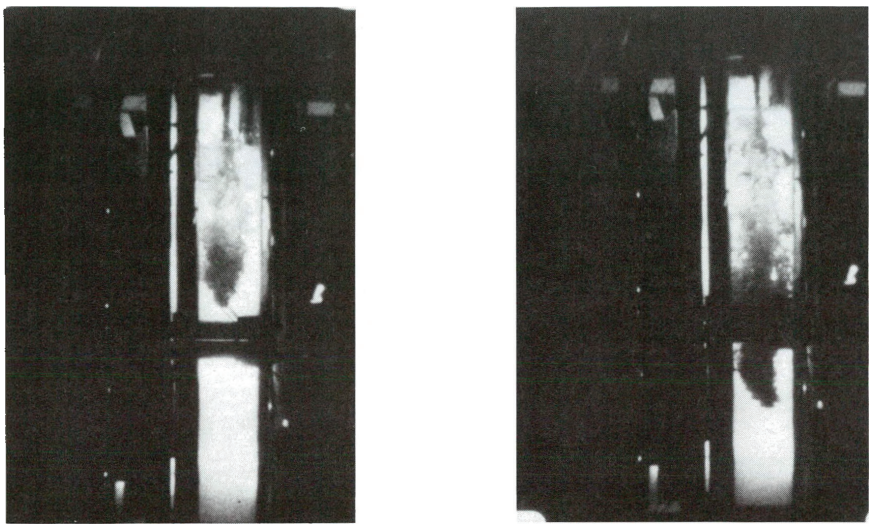

(a) t = 0.174 s, L = 0.324 m

(b) t = 0.304 s, L = 0.584 m

Figure 10. Tin Drop in Water at 100C (JC-16)

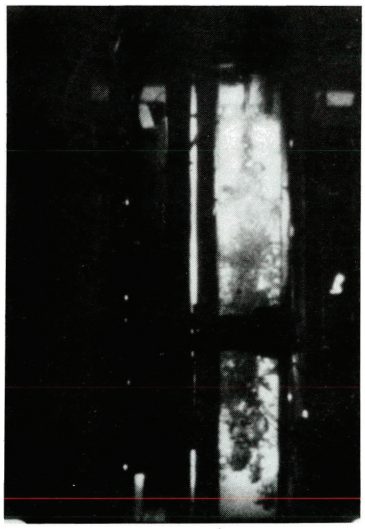

(c)

t = 0.450 s, L = 0.790 m

(d)

t = 0.294 s, L = 0.728 m

Figure 10 (cont). Tin Drop in Water at 100C (JC-16)

(a)

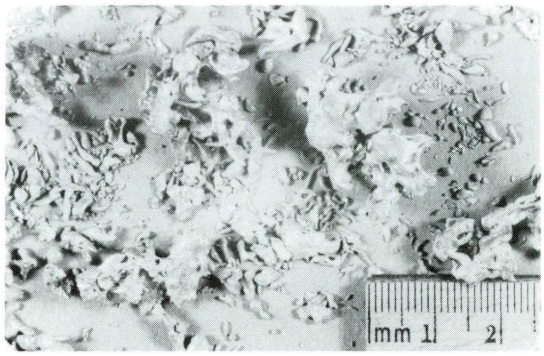

(b)

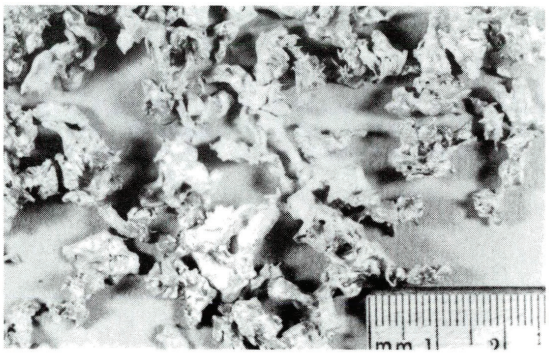

(c)

Figure 11. Particulate Material from JC-1

TABLE III. Particle Size Distributions

Run	Weight Per Cent										
	-0.425mm	+.425-.600mm	+.600-.850mm	+.850-1.00mm	+1.00-1.18mm[a] or -1.18mm	+1.18-1.41mm	+1.41-2.00mm	+2.00-2.36mm	+2.36-4.75mm	+4.75-9.5mm	+9.5mm
JC-1	-	-	-	-	2.98	1.79	5.64	4.46	35.30	40.86	8.98
JC-2	-	-	-	-	2.53	1.59	5.31	3.99	34.44	44.90	10.24
JC-3	4.36	3.46	5.01	4.42	5.34	5.66	18.39	8.54	34.83	9.54	0.45
JC-4	-	-	-	-	2.66	1.77	6.61	5.48	35.06	40.81	7.60
JC-5	2.98	3.54	5.37	5.04	5.87	7.05	17.58	10.00	35.49	6.93	0.14
JC-6	-	-	-	-	3.08	1.85	7.02	6.04	39.13	39.77	3.11
JC-7	-	-	-	-	3.16	1.90	7.47	6.51	42.03	35.79	3.14
JC-8	-	-	-	-	2.34	1.68	7.14	6.42	37.91	40.01	4.49
JC-9	-	-	-	-	2.82	1.52	5.73	4.29	30.69	44.08	10.88
JC-11	-	-	-	-	2.38	1.30	4.59	4.12	27.26	44.27	16.11
JC-17	-	-	-	-	2.05	1.36	4.63	3.64	29.11	48.33	10.88
JC-18	-	-	-	-	1.91	1.17	4.15	3.31	25.71	45.59	18.17
JC-20	-	-	-	-	2.19	1.41	5.43	4.61	31.37	44.08	10.91
JC-21	-	-	-	-	4.04	2.53	2.35	7.33	50.84	30.15	2.76

[a]This column indicates the weight per cent of particles less than 1.18 mm in size for all tests except JC-3 and JC-5.

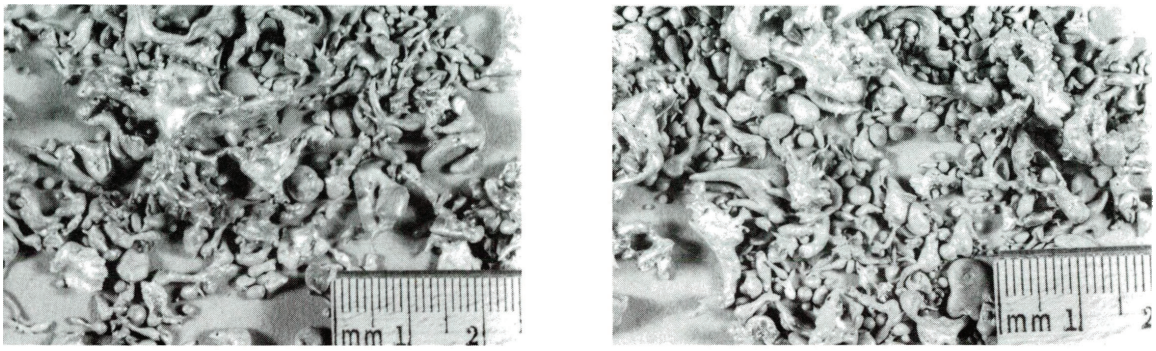

(a) (b)

Figure 12. Particulate Material from JC-4

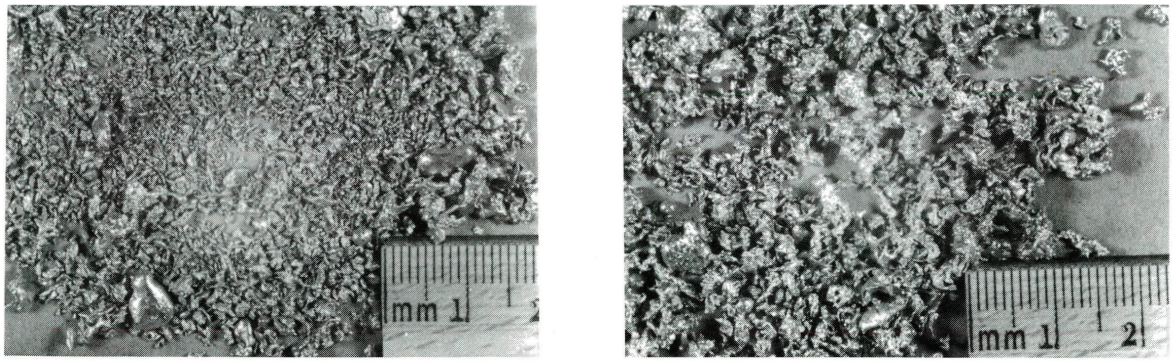

(a) (b)

Figure 13. Particulate Material from JC-5

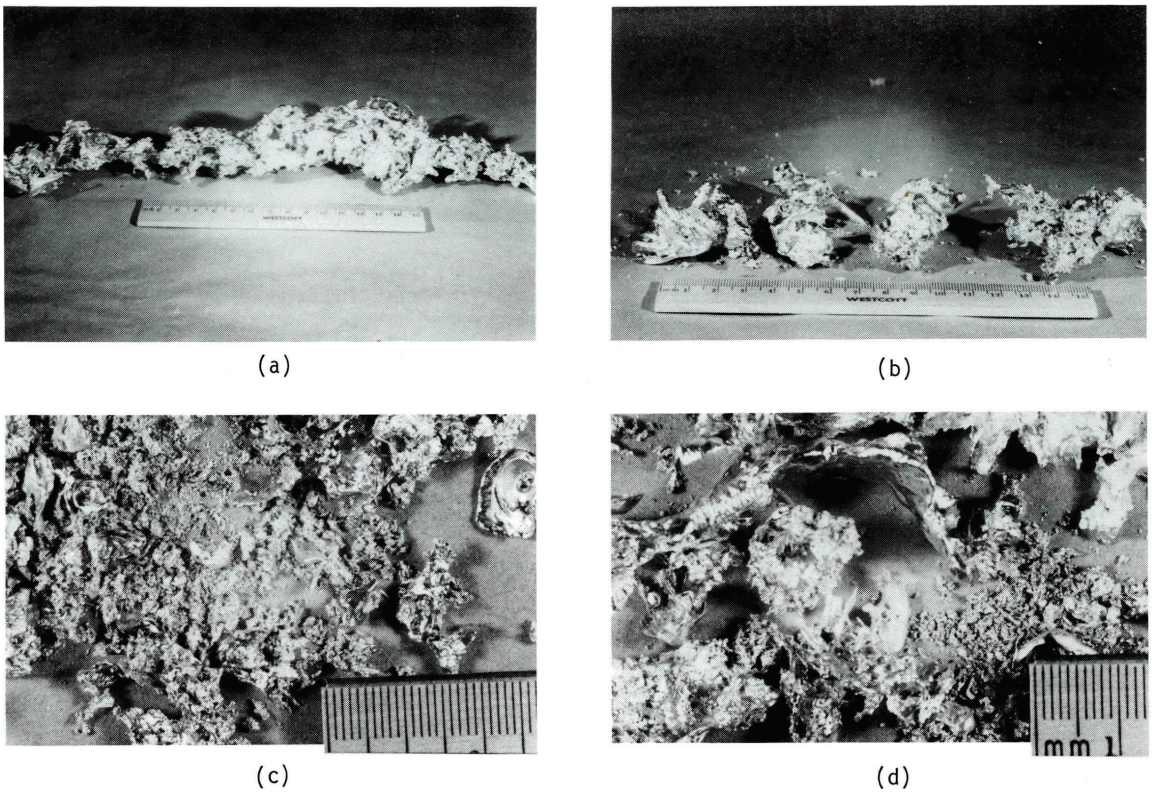

(a) (b)

(c) (d)

Figure 14. Particulate Material from JC-10

could develop. The tin particles also were spongelike with small nodules (~ 1 mm) on the surface of the larger pieces. These nodules can be attributed to nucleate boiling on the surface of the molten tin. The tin was at a high temperature (592K), and because of the higher conductivity, the interface temperature would be less suppressed when contacted with the water. This high interface temperature would cause more vigorous boiling than at the Wood's metal surface. It is also noted that the tin will solidify in water at T_{sat} whereas in the test with water at T_{sat} and Wood's metal (T_{mp} of 70C) no solid particles could be collected.

The size and shape of the solid particles depend on two important distances:

a) A distance at which the pour stream is for all practical purposes completely broken up by hydrodynamic forces into droplets of diameter less than that of the pour stream.

b) A distance at which the molten material is for all practical purposes solidified and no longer undergoing hydrodynamic deformation.

In many cases, such as in liquid metal reactors, these two distances will be essentially the same. However, if there is a high degree of superheat in the melt stream, this may not be true. Such a case could occur in a light water reactor with oxide fuel and copious vapor generation by the water.

2. Mechanisms of Breakup

The flow and breakup of the molten metal pour streams were observed to undergo several stages. These stages of typical pour stream breakup are sketched on Fig. 15.

a) Initially the pour stream exits from the drop tube and retains its cylindrical identity with little spreading. The Reynolds number based on typical test conditions for Wood's metal is initially quite high indicating turbulent flow

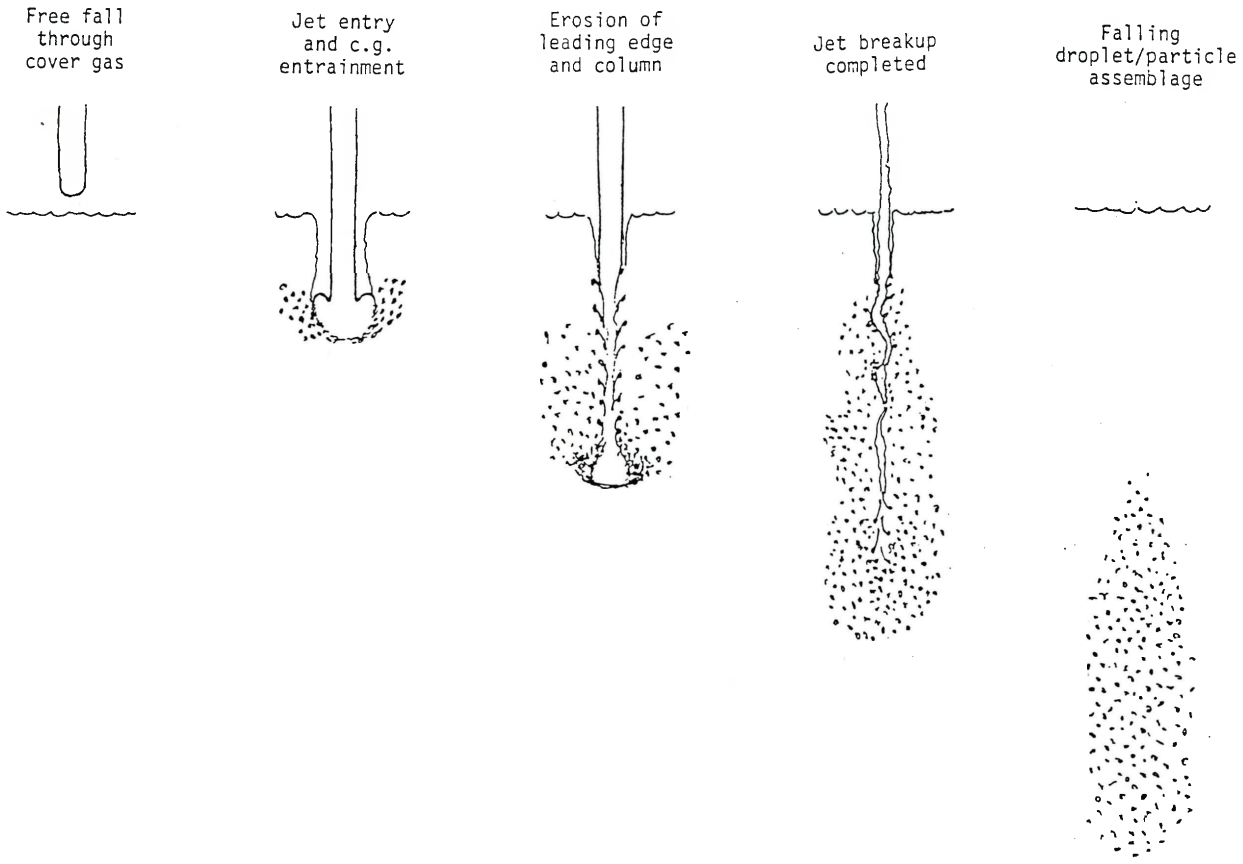

Figure 15. Stages of Typical Pour Stream Breakup

$$\frac{D_{ji} U_j \rho}{\mu} = \frac{(0.025)(2)(9200)}{(1.6 \times 10^{-3})} = 2.9 \times 10^5$$

b) The pour stream then impinges into the water causing lateral and reverse flow of the leading edge of the pour stream. This flow is illustrated in the sketch on Fig. 16. This impingement flow has been analyzed by Hopkins and Robertson[25] for two dimensions. This flow is captured in the mushrooming shape of the leading edge, which is ~ $2D_{ji}$, in the motion picture photographs (see Fig. 5b) and in the frozen leading edge recovered from test FFC-2 with uranium in sodium (Fig. 17).[23]

This impingement of the pour stream causes spreading and thinning of the leading edge resulting in sheet formation of the fragments during freezing. Filaments are also formed by the surface tension force reducing the surface area of the sheets. As the metal cools the viscosity will undergo drastic changes affecting the flow behavior of the pour stream. Flow on the outer surface is arrested after freezing occurs and progresses inward after the pour stream has contacted the cooler water.

c) Mixing of the fragments formed from the pour stream impingement with the water forms a zone which spreads laterally. This initial mixing is shown in Fig. 4e for test JC-20. This initial mixing zone before it progresses downward is a region for subsequent jet breakup with mean properties different from that of only the water. This behavior was also observed by Marshall and Berman.[26]

d) As the initial mixing zone moves downward the leading edge breakup is influenced only by the water (Fig. 4f) and breakup occurs from instabilities described by previous workers for continuous jets. Figure 4d is a photograph showing breakup development of the pour stream along the trailing column. Material is stripped off the walls of the pour stream by a

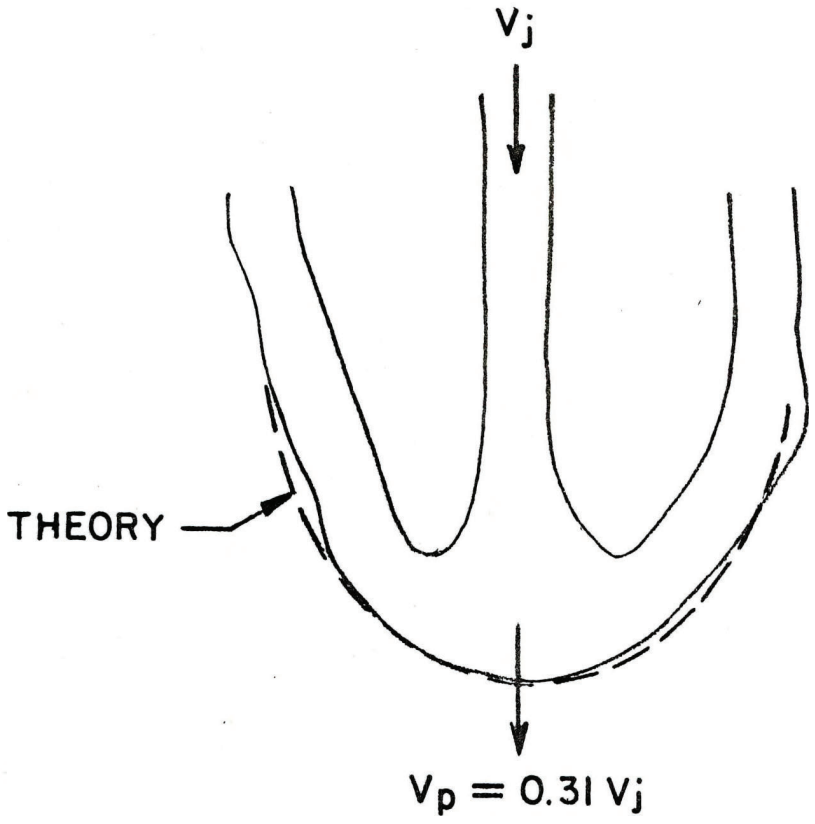

Figure 16. Impingement Flow of Leading Edge

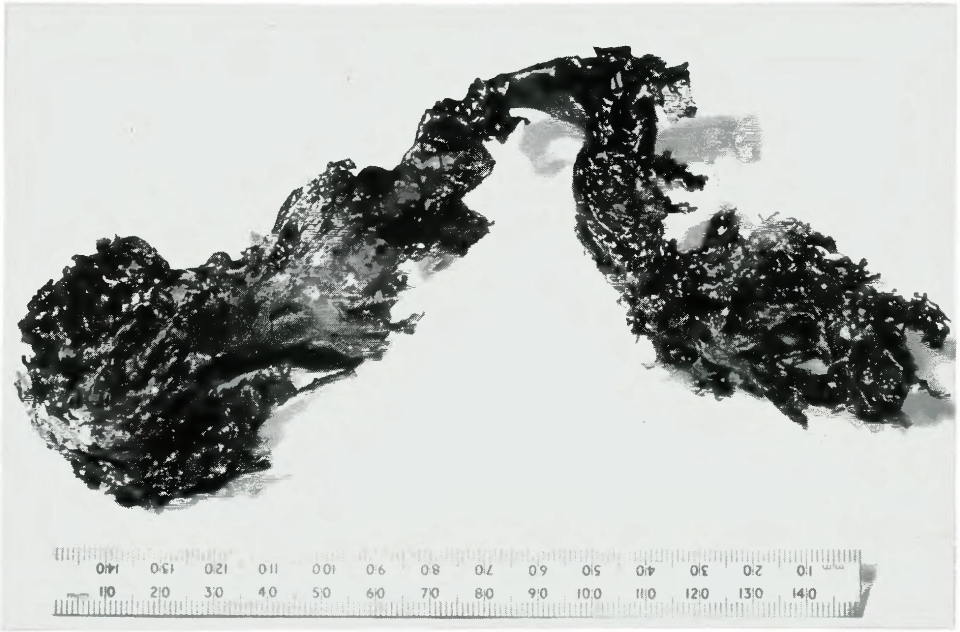

Figure 17. Frozen Leading Edge from Test FFC-2[23]

Kelvin-Helmholtz type instability. The undulations which are stripped off in the form of what is termed shearing puffs by Reynolds are sketched on Fig. 18. For small diameter (~ 1 mm) jets in laminar flow these type of varicose undulations develop into drops of diameter approximately equivalent to that of the jet. As long as the high-velocity central core feeds into the leading edge region, the leading edge velocity (penetration rate) remains high, reflective of the core velocity. When the core becomes fully depleted, the leading edge velocity is that of gravity settling of the particles formed by the breakup.

Sinuous wave formation is another form of instability that results in jet breakup. A slight sinuous movement of the pour stream can be seen while material is being stripped off its surface in Fig. 4c. This sinuous motion can develop into what has been referred to as pedal breakdown by Reynolds[24] (see Fig. 19). This type of breakdown is shown in the photograph on Fig. 20 of the frozen pour stream of uranium - 5 w/o zirconium alloy in test FCC-5. In FCC-5 the uranium alloy was heated only 10C above its liquidus point (1524K) and portions of the pour stream were frozen before breakup. Breakdown of the points where the pour stream changes direction is seen from the photograph. No explanation either theoretical or qualitative was given for this behavior by workers who observed similar behavior for upward jet flow.[24,27] Apparently a localized mixing zone is formed at the leading edge of the pour stream which diverts the flow. The pour stream then begins to buckle and at the breaks further pour stream dissipation begins. This apparently is the pattern in the frozen pour stream seen in the radiograph for test FFC-5.

3. Size of Mixing Zone

Measurements were made from the motion picture film of the apparent diameter of the mixing zone as a function of pool depth and time. The mixing zone was taken to include the metal particles and drops, vapor/gas, and jet

Figure 18. Undulations being Stripped off According to Reynolds[24]

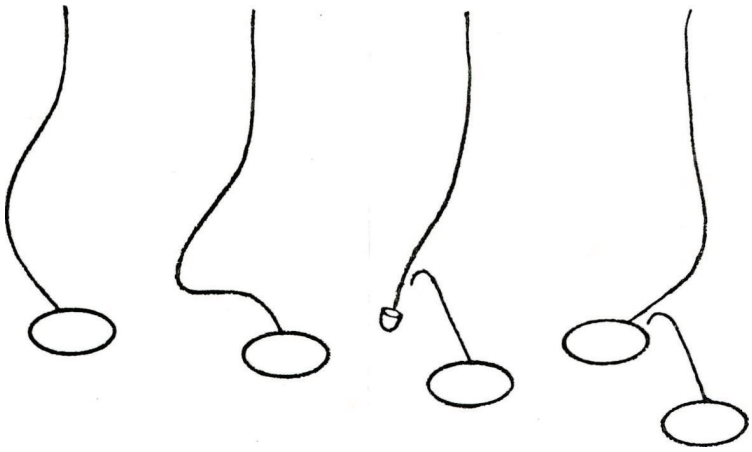

Figure 19. Pedal Breakdown According to Reynolds[24]

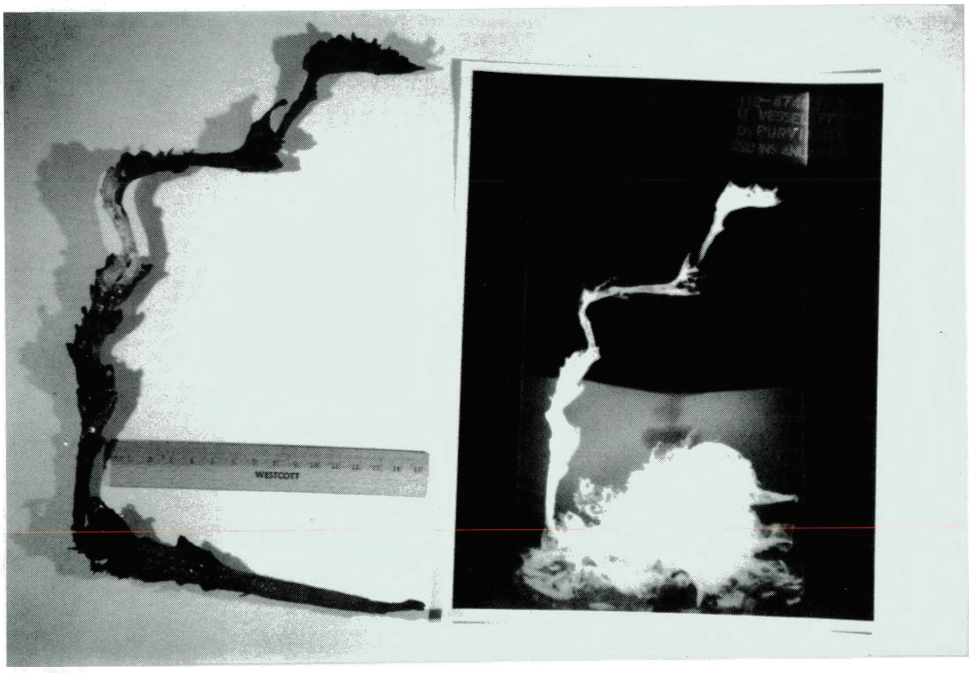

Figure 20. Frozen Jet Column Recovered from Test FFC-5[23]

core. The annular space surrounding the mixing zone was clear water. Position H = -127 mm is above the water-cover gas interface and therefore indicates the free pour stream diameter.

Figure 21 shows the results of JC-15 (tin at 580K into water at 298K). In this test the mild explosive interactions caused the mixing zone to rapidly expand to the vessel diameter. In test JC-16 (tin at 568K into water at 373K) no explosive interactions occurred, but the steam bubbles created by the rapid boiling resulted in eventual expansion of the mixing zone at the lower depths to the diameter of the glass container (Fig. 22).

The mixing zones for representative Wood's metal tests are shown in Figs. 23 to 30. Except for JC-24 and 31, the Wood's metal temperature was relatively low (359 to 400K) and the mixing zone did not extend to the walls of the glass column. In tests JC-24 and 31 with the Wood's metal at 718K and 500K and the water at saturation (373K), vigorous boiling occurred resulting in significant expansion of the mixing zone diameter. However, it is interesting to note that the mixing zone diameter was generally smaller in JC-19 with the water at 373K than in JC-20 with the water at 298K. With the water at 373K the Wood's metal did not freeze but tended to form spherical globules with a higher terminal velocity than the irregularly shaped frozen fragments formed in the test with the water at 298K. This resulted in more rapid settling and reduced lateral dispersion. Because the Wood's metal was at a low temperature (378K and 389K) in these tests reduced vapor generation occurred. This phenomenon is also seen in the comparison of the mixing zones for tests JC-28 and 29.

The expansion of the mixing zone in the Wood's metal tests JC-30 and 32 was similar to that for the tin test JC-16. The metal melt was relatively hot in these tests (> 573K) resulting in increased vapor generation and progressively increasing mixing zone expansion as the pour stream material moved deeper in the water pool.

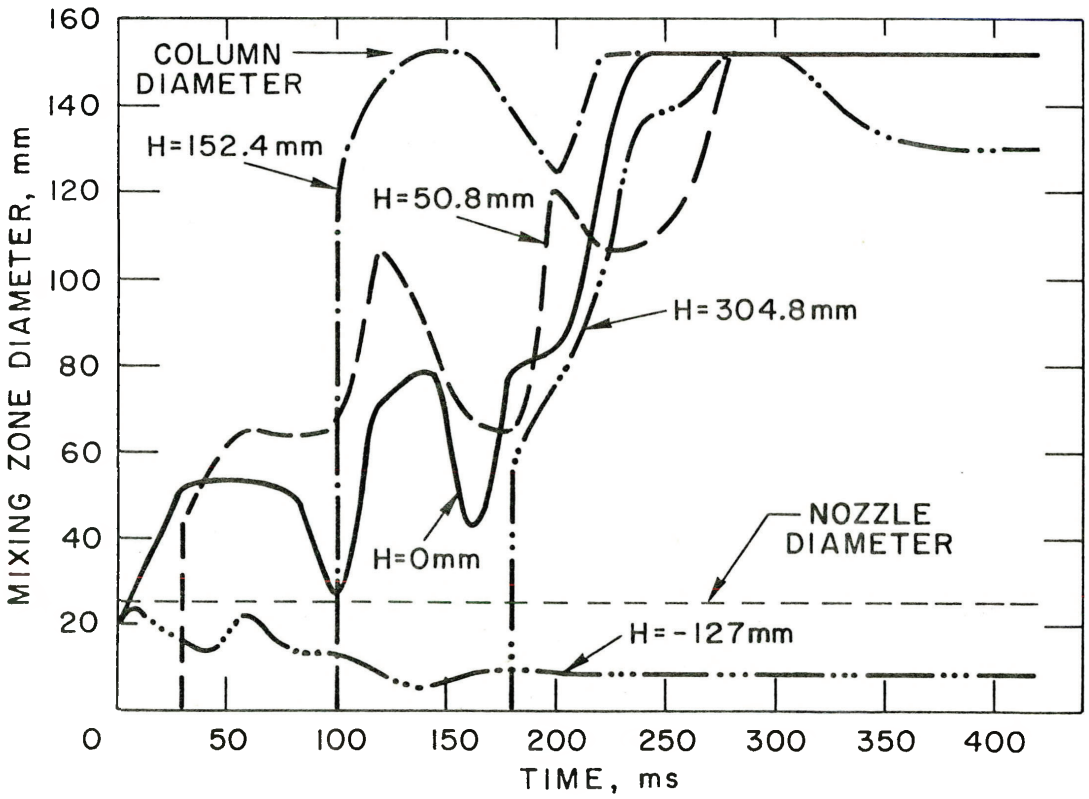

Figure 21. Mixing Zone Diameter for JC-15
(Tin - 298K Water)

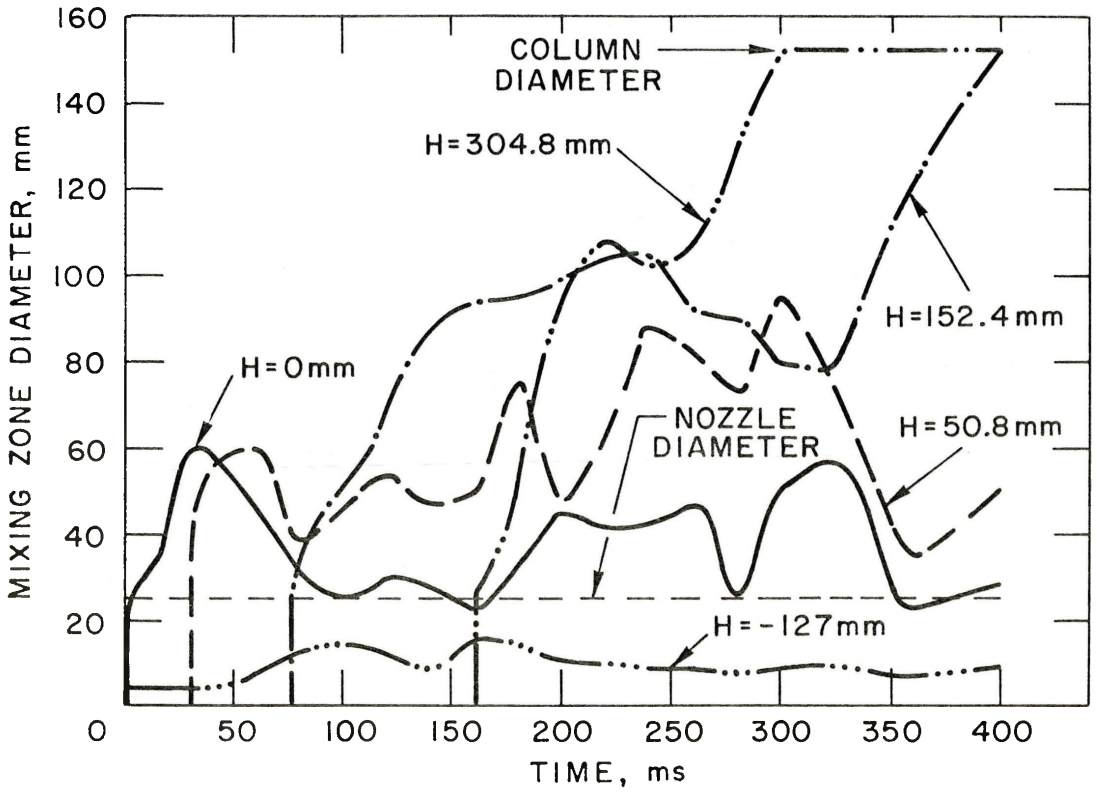

Figure 22. Mixing Zone Diameter for JC-16
(Tin - 372K Water)

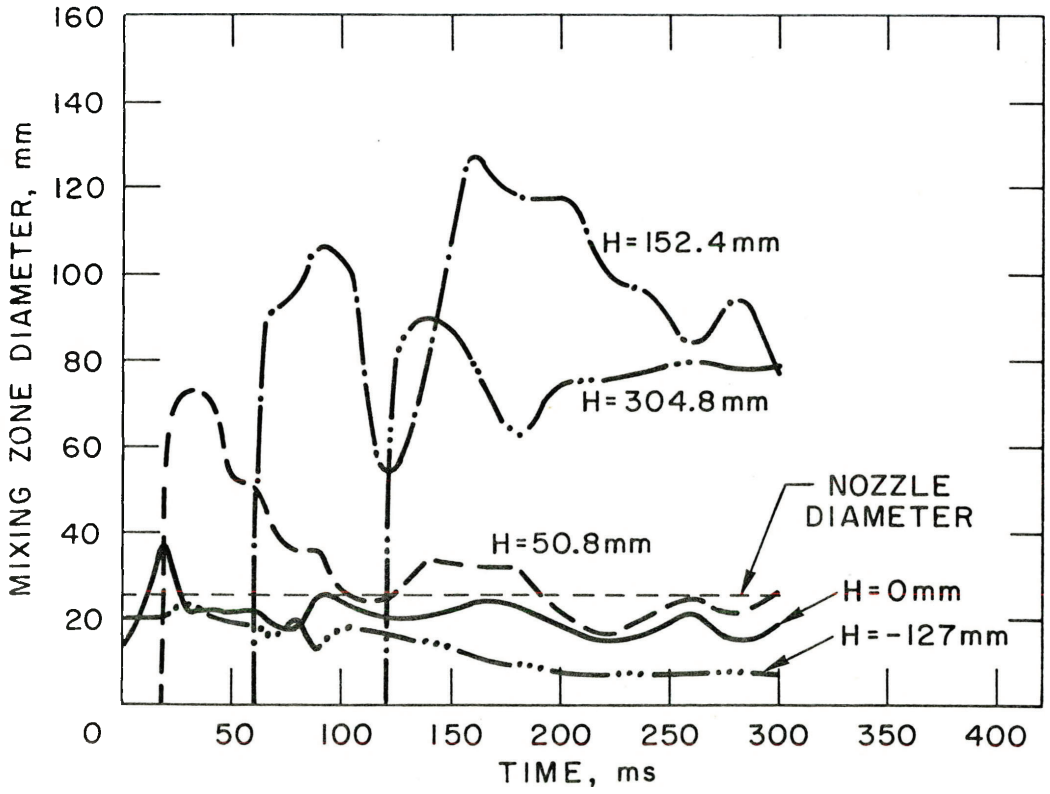

Figure 23. Mixing Zone Diameter for JC-19
(389K Wood's Metal - 373K Water)

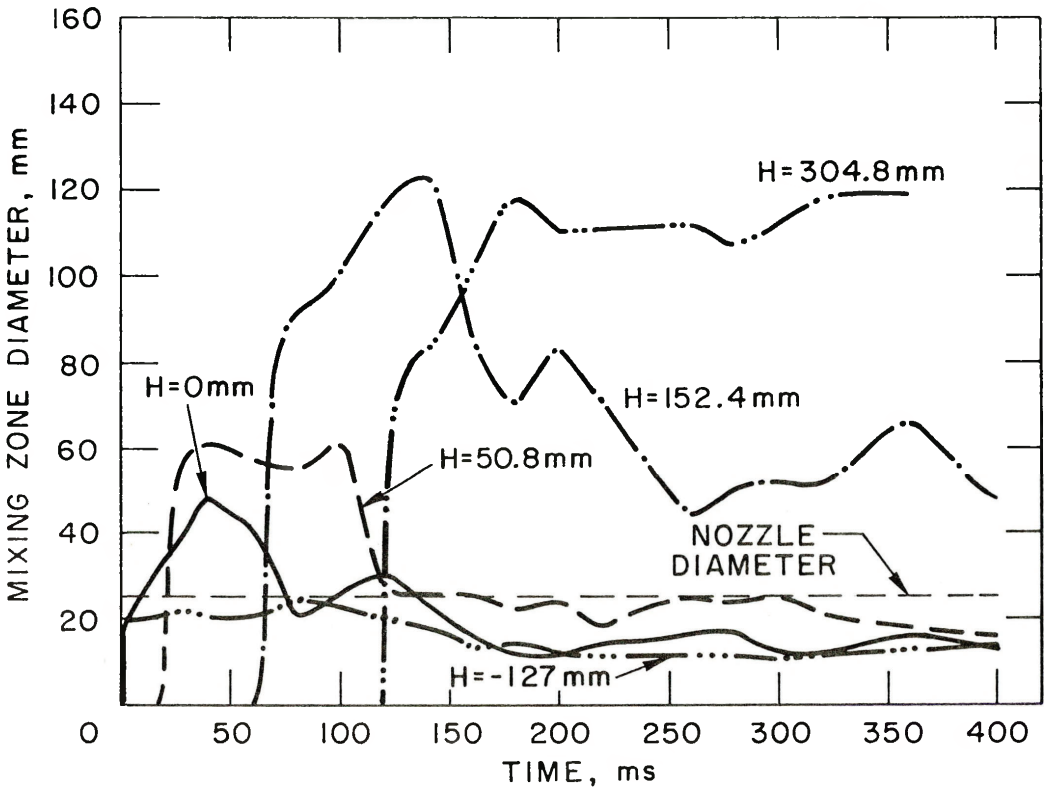

Figure 24. Mixing Zone Diameter for JC-20
(378K Wood's Metal - 298K Water)

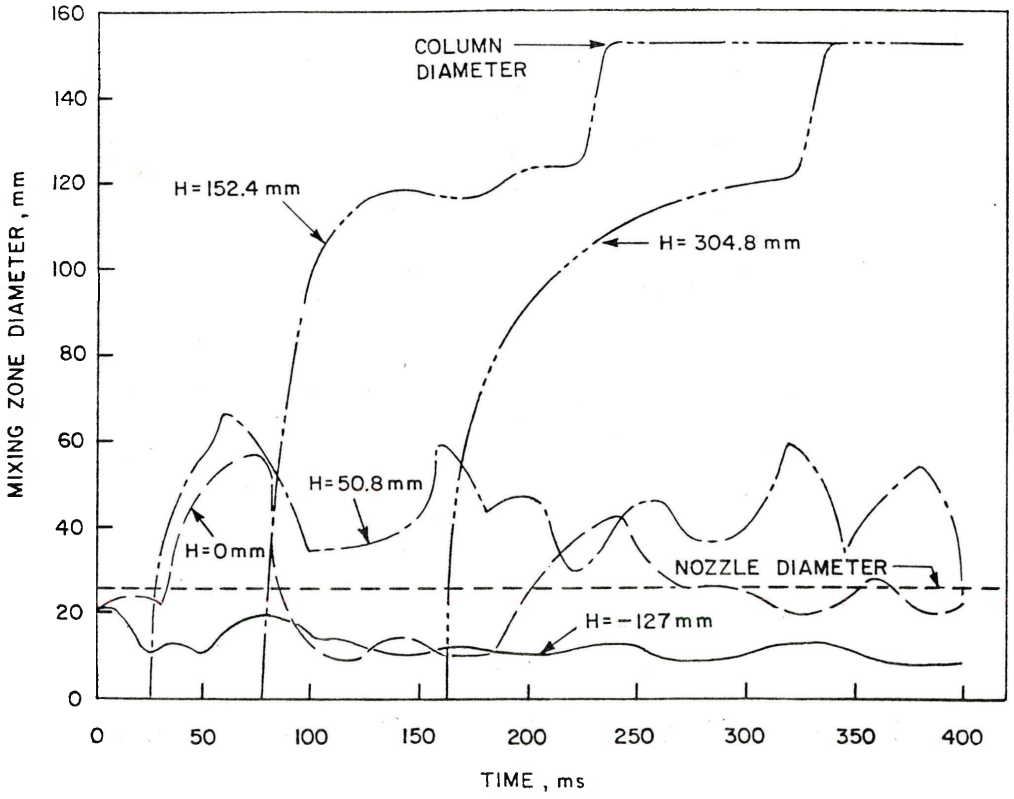

Figure 25. Mixing Zone Diameter for JC-24
(718K Wood's Metal - 372K Water)

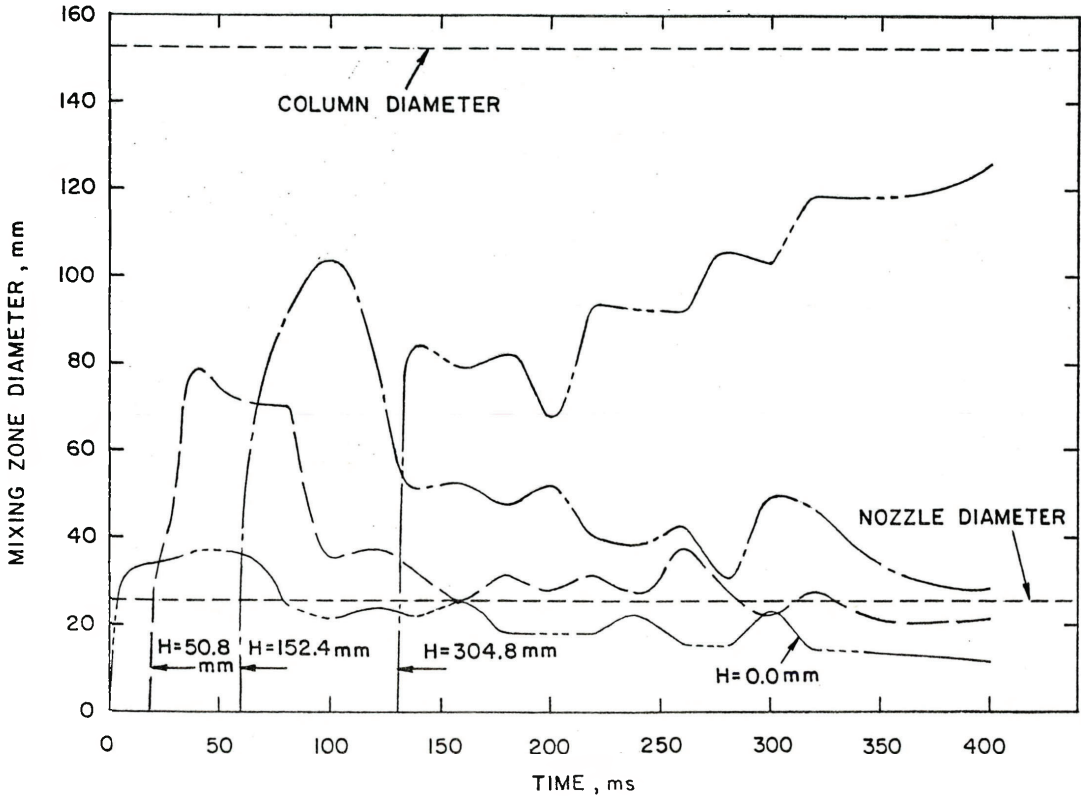

Figure 26. Mixing Zone Diameter for JC-28
(373K Wood's Metal - 296K Water)

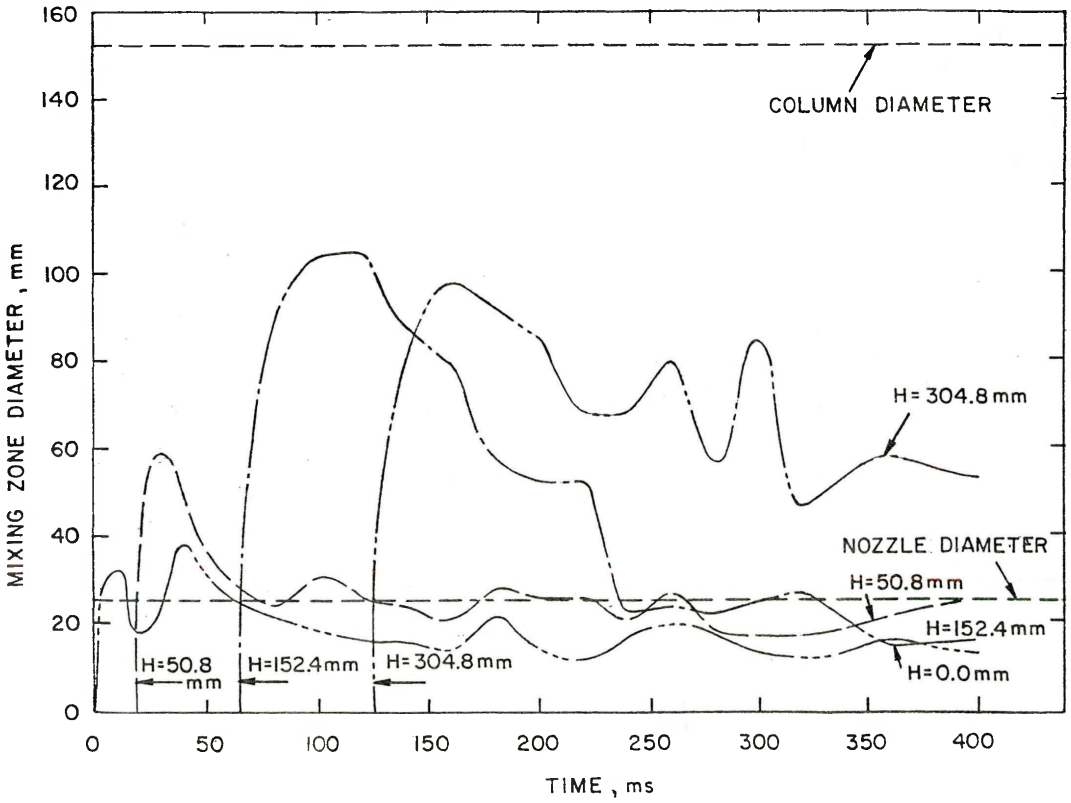

Figure 27. Mixing Zone Diameter for JC-29
(400K Wood's Metal - 373K Water)

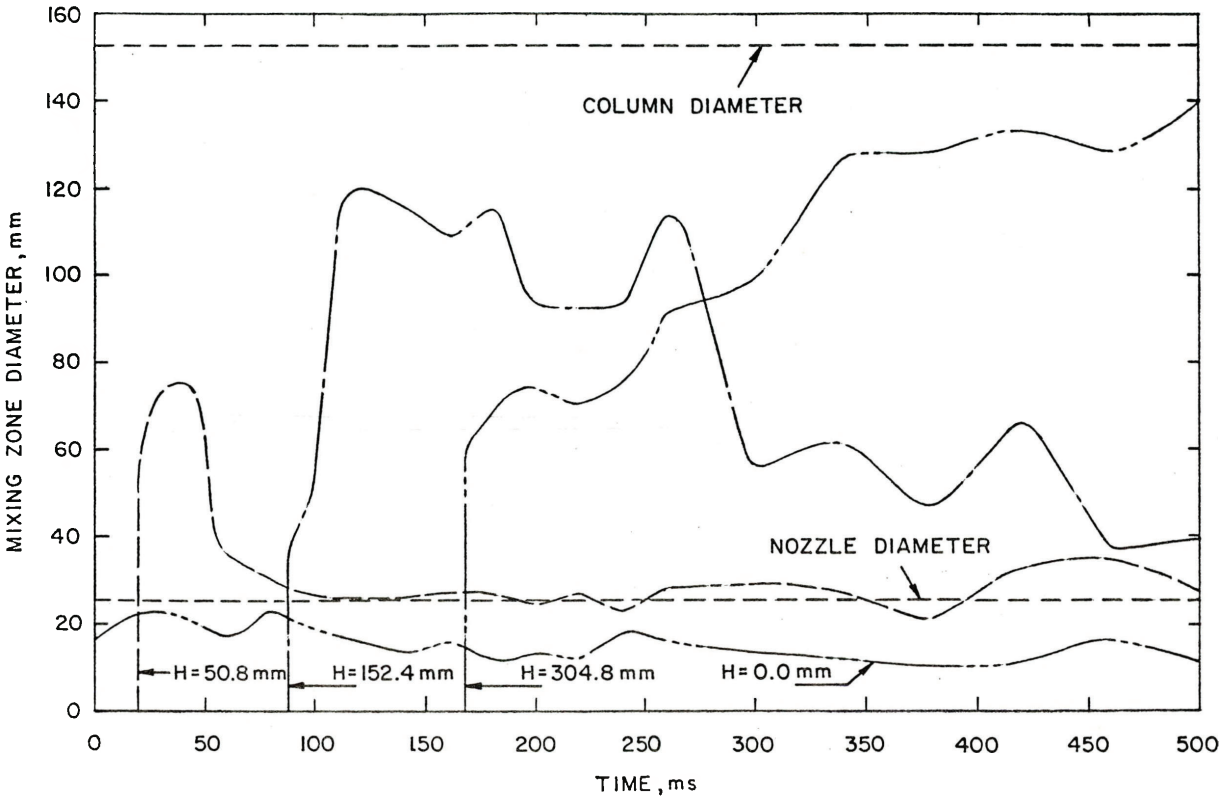

Figure 28. Mixing Zone Diameter for JC-30
(472K Wood's Metal - 292K Water)

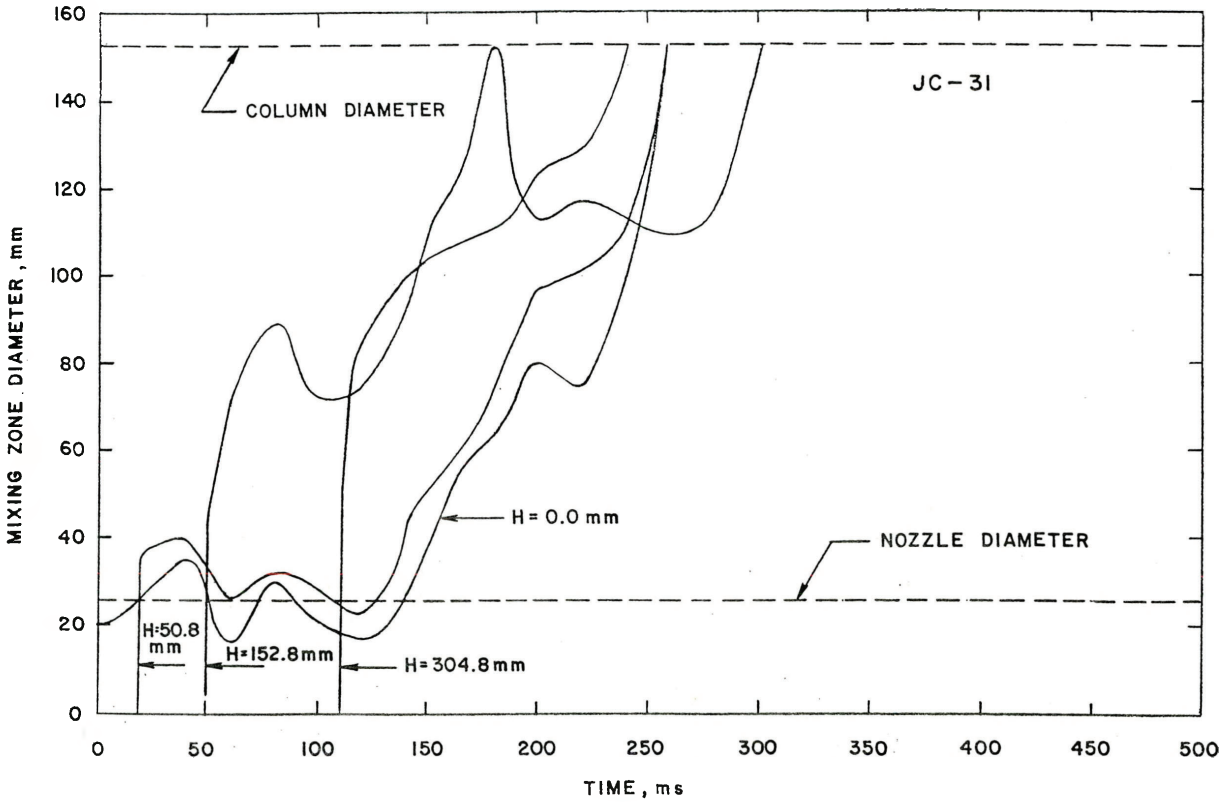

Figure 29. Mixing Zone Diameter for JC-31
(582K Wood's Metal - 373K Water)

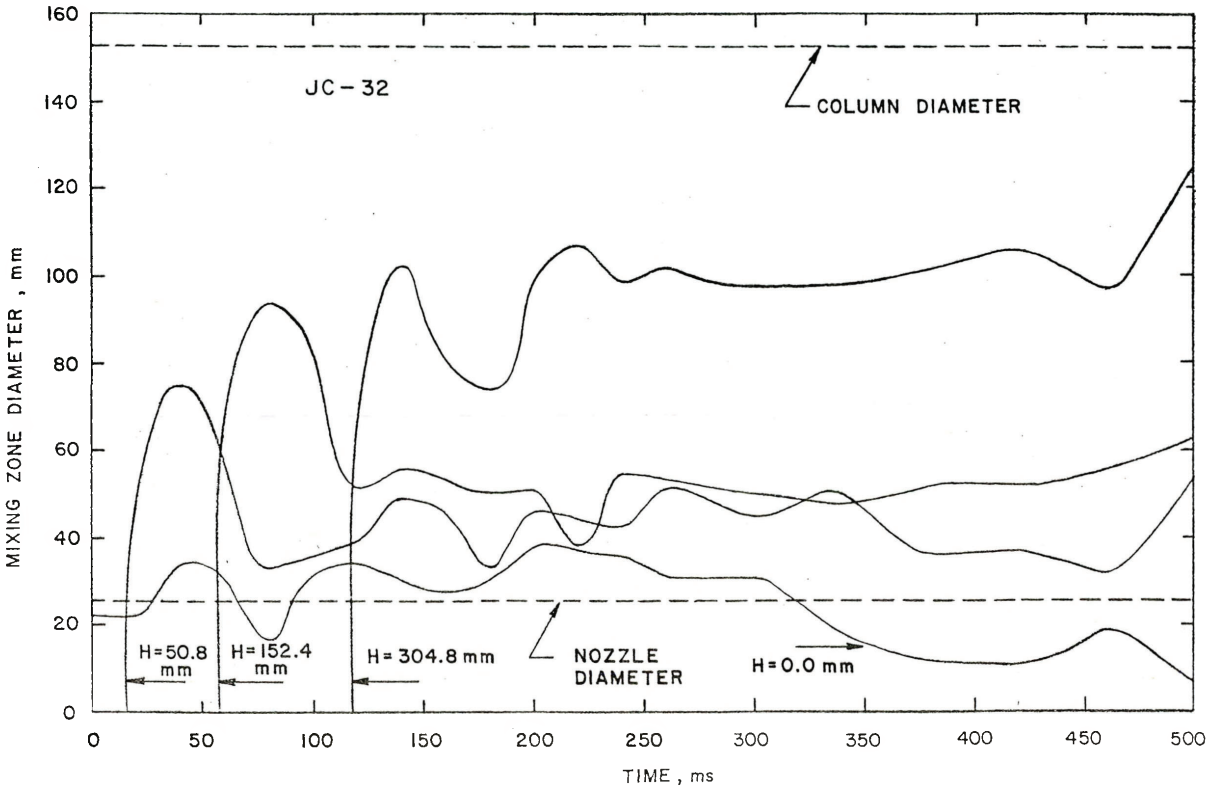

Figure 30. Mixing Zone Diameter for JC-32
(496K Wood's Metal - 296K Water)

4. Leading Edge Velocity

The position of the leading edge as a function of time was determined from the motion picture films. The behavior of the leading edge velocity can be used to interpret the breakup process. The leading edge velocity is reflective of the core velocity as long as the central core feeds into the leading edge region. When the core is depleted, the leading edge velocity is the settling velocity of the particles formed by the breakup. The position, L, of the pour stream leading edge for test JC-23 normalized in terms of the initial pour stream diameter, D_{ji}, plotted on Fig. 31. This experiment in which no water was in the glass container and the pour stream was dropped in air was conducted for comparative purposes with drops in water and can also be considered as an extreme case of film boiling in which the pour stream is surrounded by a vapor blanket. The pour stream position is compared with that for gravitational acceleration. The initial pour stream velocity was greater than that for gravitation acceleration because the injector/furnace was somewhat pressurized to 21 KPa. After the pour stream had attained a position of about 10 stream diameters, the slope of the L/D_{ji}-versus-time curve parallels that of the gravity curve indicating that the pour stream was affected primarily by gravity at that point.

Figure 32 is a plot of the leading edge velocity for tests with the water subcooled (room temperature) so that there would be essentially no effect of steam generation. Tests JC-20 and 28 were with the pour stream at the boiling point of water. The cover gas was air (noncondensable) for JC-20 and steam (condensable) for JC-28. The pour stream penetration rates show that JC-20 and 28 were almost identical, indicating no overall effect of entrainment of a condensable vs. a noncondensable cover gas. At about $L/D_{ji} = 20$, both sets of data show a slowing down of the leading edge interpreted here as indication of the pour stream breakup distance. Rather than an abrupt decrease in penetration velocity as the leading edge changes from high-velocity influx to particle settling, the decrease is seen to be gradual, indicating reduction in particle-to-particle interaction as the particle field spreads laterally. The settling velocity becomes constant beyond $L/D_{ji} = 25$. For JC-20 the constant settling velocity was 0.82 m/s. The effect of particle concentration on settling velocity is discussed in Appendix B.

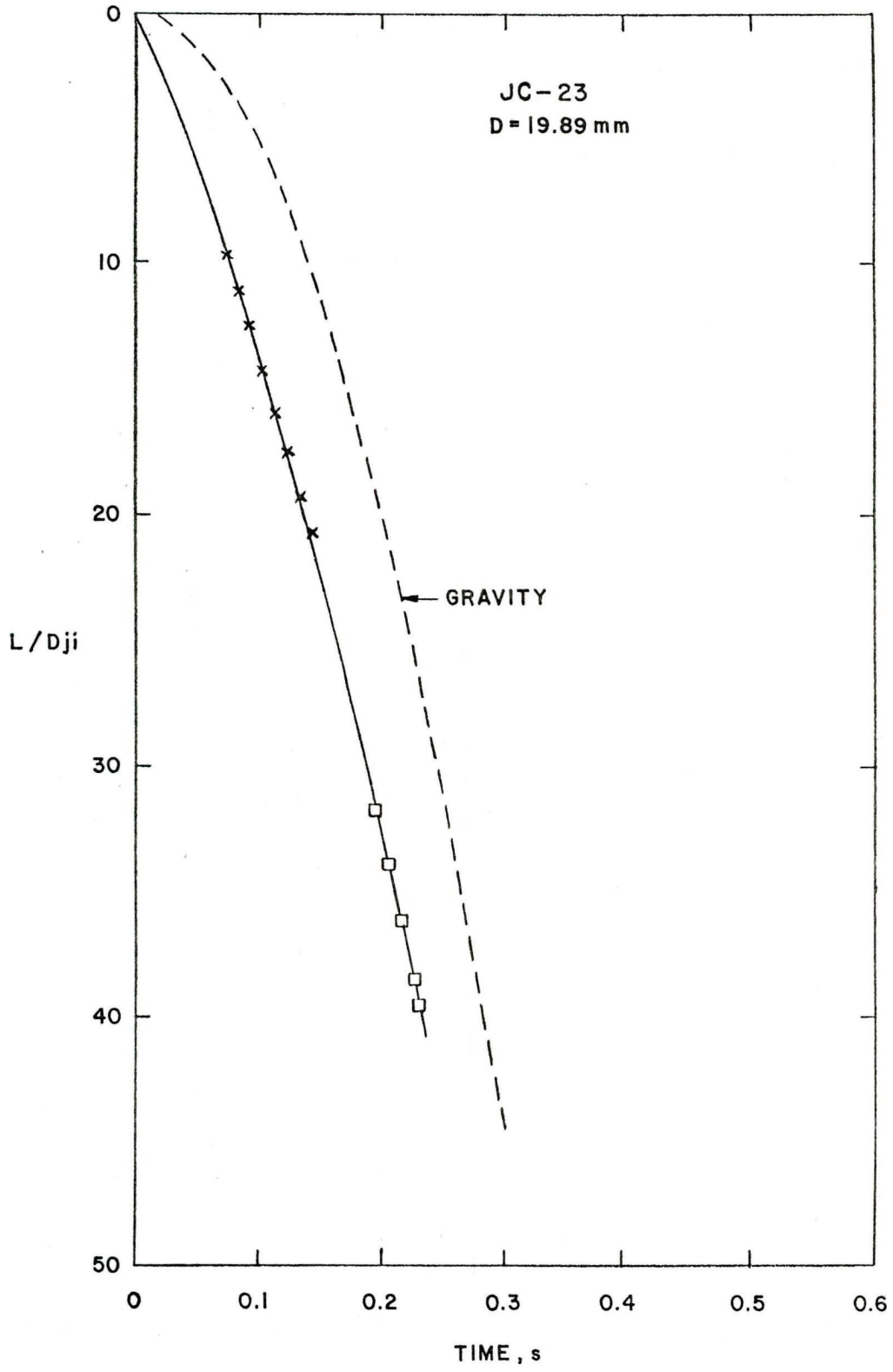

Figure 31. Comparison of Leading Edge Position for Pour Stream Drop in Air (JC-23) with that by Gravitational Acceleration

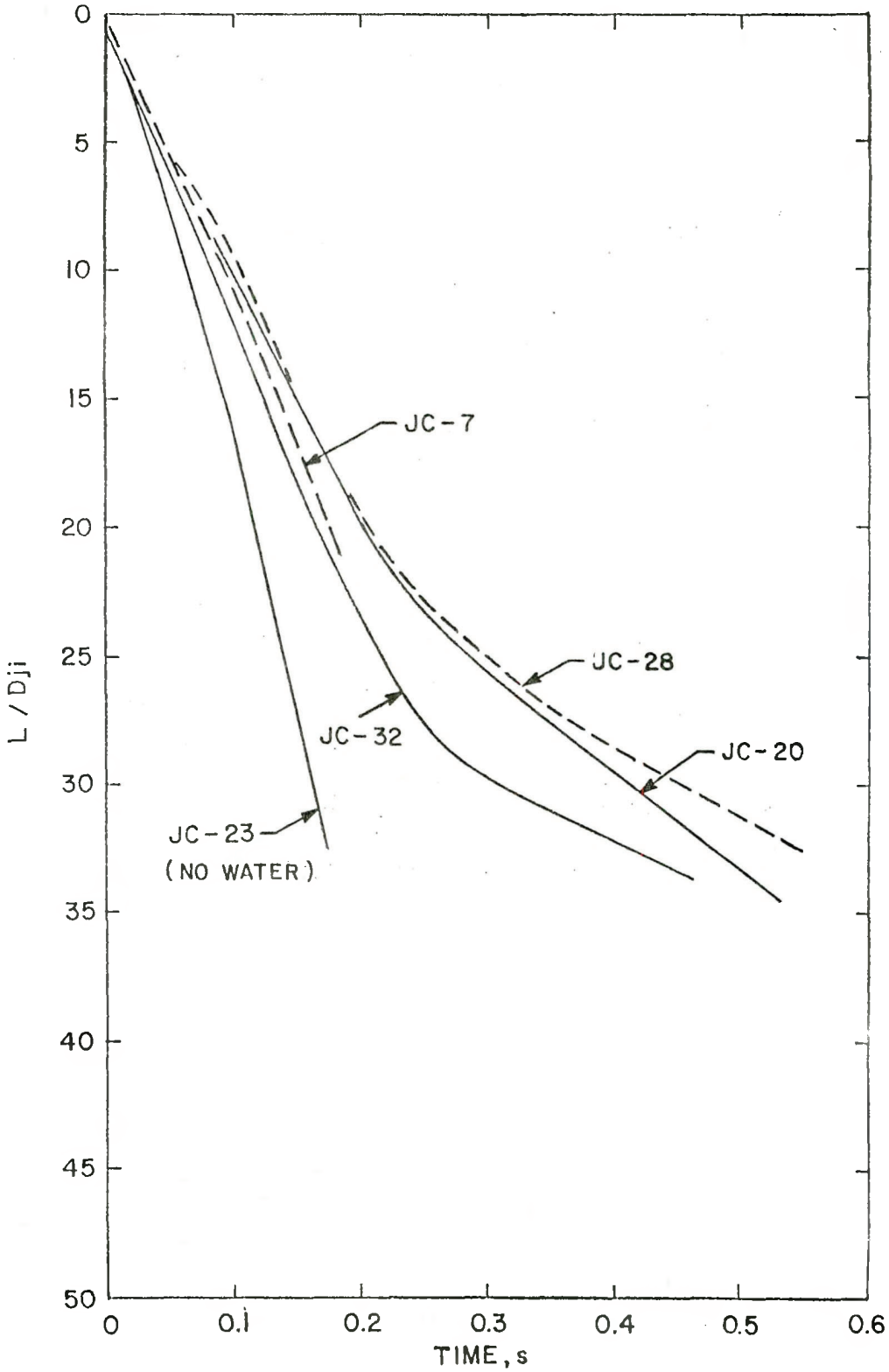

Figure 32. Leading Edge Velocities with Subcooled Water

Tests JC-7 and 32 were conducted with higher melt temperatures to attain local boiling at the pour stream/water interface. The initial pour stream penetration velocities for JC-7 and 32 were essentially the same. However, the camera view for JC-7 did not extend deep enough into the pool to determine the breakup distance. The breakup distance for JC-32 was about a L/D_{ji} = 25, somewhat longer than for JC-20 and 28. While there was no large-scale steam generation because of the subcooled water, some effect is indicated by the increased pour stream breakup length.

For comparison, the penetration distance as a function of time for JC-23, the pour stream drop in air, is shown in Fig. 32.

Four tests, JC-19, 29, 13, and 24 (in order of increasing melt temperatures), were conducted with the water at its boiling point. There were no solid particles of Wood's metal (T_{mp} 70C) formed at the 100C system temperature. The penetration behavior was quite different than the tests without steam generation (see Fig. 33). The initial penetration rates for tests JC-24 and 29 were comparable to test JC-29 for pour stream free fall through air. The camera views for JC-13 and 19 were insufficient to observe their break points. For JC-29 the break occurred at L/D_{ji} = 43. There was no observable break point for JC-24 in the experimental pool depth (L/D_{ji} = 50).

Figures 34 and 35 are plots of localized rather than average velocity as a function of position. On Fig. 34 are the leading edge velocities for the tin tests JC-15 and 16. In both of these tests the melt temperature was high resulting in considerable boiling on the melt stream surface and particularly for JC-15 where the water was at saturation (373K). For the most part the pour stream in JC-15 was blanketed by water vapor resulting in less resistance to the flow of the melt material and a fairly uniform velocity. The leading edge velocity did tend to decrease deeper into the water pool. In test JC-16 with the water at 298K minor explosions occurred resulting in rapid acceleration particularly in the region of 0.05 to 0.045 m below the initial water level. These interactions formed finer particles which finally settled at a much lower velocity than the fragments of JC-15.

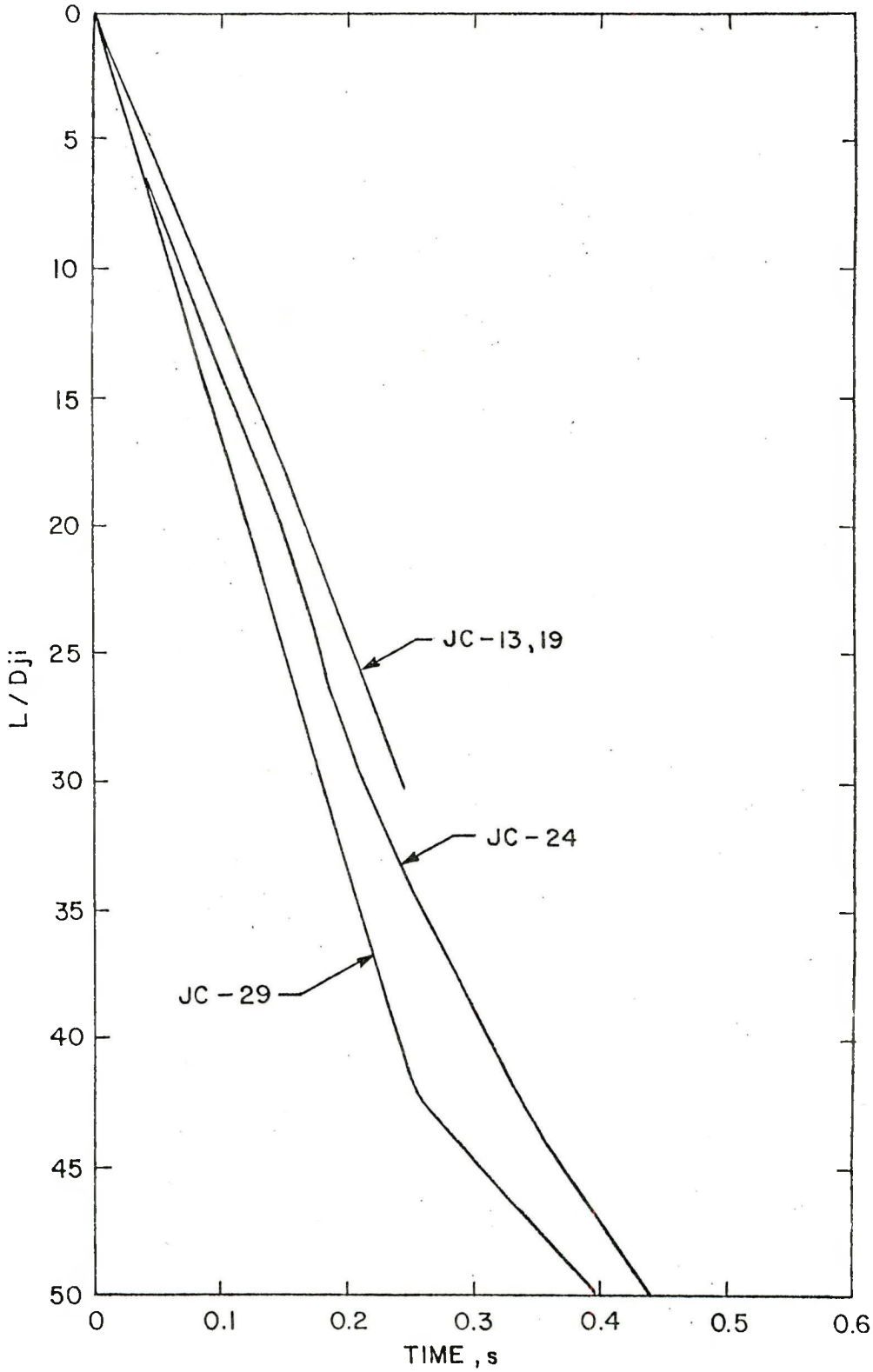

Figure 33. Leading Edge Velocities with Saturated Water

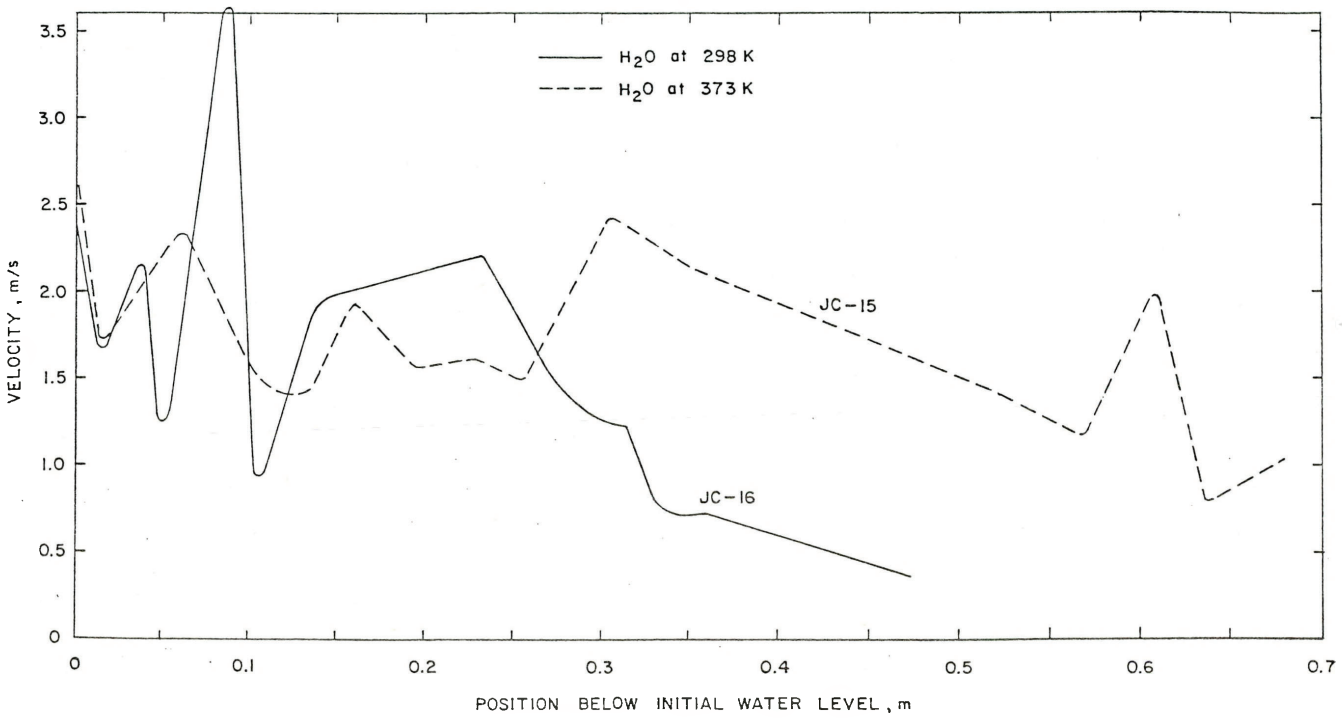

Figure 34. Localized Leading Edge Velocities for JC-15 and -16 (Tin)

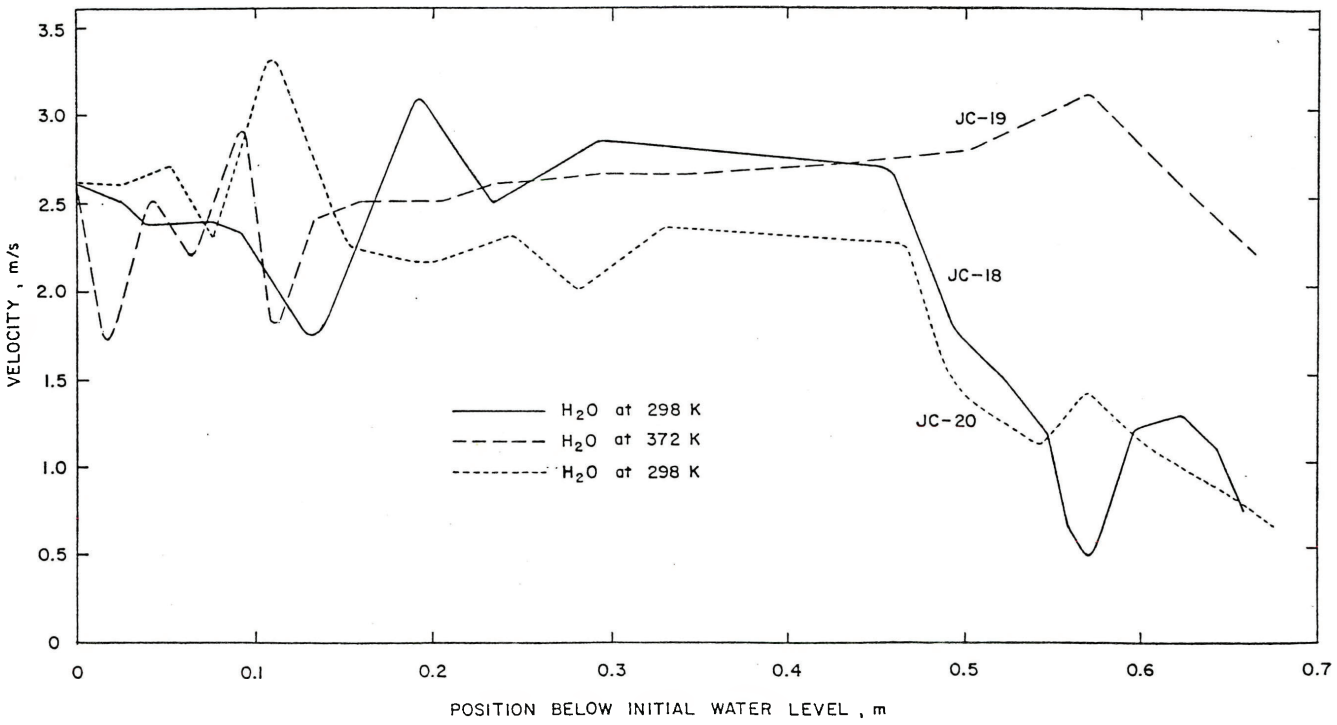

Figure 35. Localized Leading Edge Velocities for JC-18, -19, and -20 (Wood's Metal)

On Fig. 35 are plotted the leading edge velocities for tests JC-18, -19, and -20 with Wood's metal. The melt temperatures for these tests were essentially the same (ranging from 105 to 123C). The water temperature for JC-18 and -20 was at room temperature (25C), and the corresponding velocities were about the same even though the cover gas was air for JC-19 and steam for JC-20 indicating little effect by the entrained air. The water temperature for JC-19 was at T_{sat} generating more boiling than for JC-18 and -20. The increased voidage in the water caused by the vapor bubbles reduced the drag on the melt material resulting in a higher velocity at 0.5 m and deeper than for JC-18 and -20.

The oscillations in the velocity in all of the tests can be attributed to the complex interaction of the jet material, surface boiling, and water flow.

5. Pool Swell

In these experiments the melt passed through 150 mm of cover gas prior to entering the water. In eight experiments the cover gas was steam from the vaporization of the water pool at saturation temperature (100C). For the tests with water at room temperature the cover gas was air except for the tests in which the air was purged by steam from an external steam generator.

An indication of the amount of cover gas entrained can be obtained from the change in level of the water surface. The volume of the entrained air and the vapor generated by the molten metal jet was obtained by subtracting the volume of the melt from the total swell volume. A comparison of the volumetric increase of the pool between JC-18 and JC-20 is shown on Fig. 36. In JC-18 the cover gas above the pool was air and the swell is attributed to both steam generation by the hot melt and entrained cover gas and therefore is greater than for JC-20 in which the cover gas was condensible steam. The melt was at a low temperature (123 and 105C) for these two tests. In JC-32 with air cover gas the melt temperature was increased to 223C resulting in additional boiling and increased and sustained swell volume. The dip in the curves on Fig. 36 is attributed to disengagement of the entrained cover gas followed by vapor buildup in the lower sections of the pool as the heat is being transferred from the pour stream.

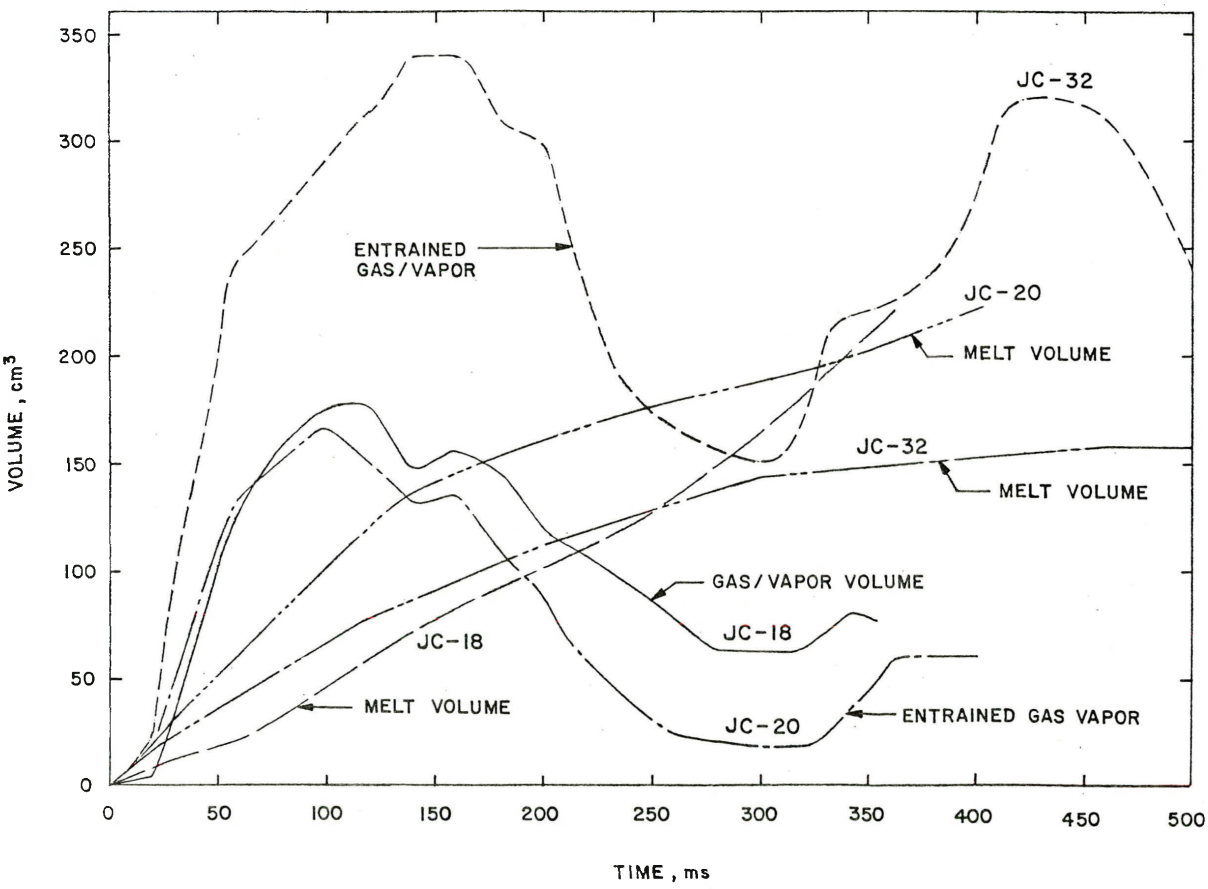

Figure 36. Pool Swell for JC-18, -20, and -32

Figure 37 shows the pool swell caused by vapor generation for JC-24, -29, and -31. In these tests the water was at 100C and all heat transferred from the melt was converted into water boiling. In JC-31 the Wood's metal temperature was higher (310C) than in JC-29 (101C) and this is reflected in the increased swell volume. At 220 ms the swell filled the entire freeboard space to overflow and was no longer measurable. However, the swell volume was less for JC-24 than for JC-31 even though the Wood's metal temperature for JC-24 (445C) was much higher than for JC-31. In JC-24 the water was essentially film boiling on the Wood's metal pour stream resulting in reduced heat transfer and hence reduced vapor generation in comparison with JC-31 in which nucleate boiling and a higher heat transfer rate occurred. The boiling rate for JC-24, however, did exceed that of JC-29 with the lowest melt temperature.

Figure 38 shows the swell volume for two tests (JC-15 and 16) in which tin was used for the melt material. In test JC-15 with the water at 25C a minor explosion occurred resulting in the volume spike. There was no explosion observed in JC-18 but because the water was at saturation (100C) significant steam generation occurred resulting in a steady but large increase in vapor volume.

Estimates were made of the void fraction within the mixing zone from the swell data for JC-24 and JC-31. It is believed that film boiling occurred in JC-24 (Wood's metal at 445C) to blanket the pour stream and reduced the heat transfer and therefore vapor generation rate. While the Wood's metal was relatively hot (310C) in JC-31, film boiling did not occur but vigorous nucleate boiling resulted which generated large quantities of steam. It was assumed that the mixing zones were radially symmetric and the swell volume was a measure of the vapor and melt volume. The estimated void fractions of the mixing zones for these two tests are tabulated in Table IV as a function of leading edge position below the initial water level. The void fractions are defined as vapor volume divided by the mixing zone volume (consisting of vapor, water, and melt).

The voidage for JC-24 ranges from 0.25 to 0.44 and from 0.84 to 0.93 for JC-31. Although the voidage of the vapor blanket for film boiling in the immediate vicinity of the pour stream would be much greater than that for film

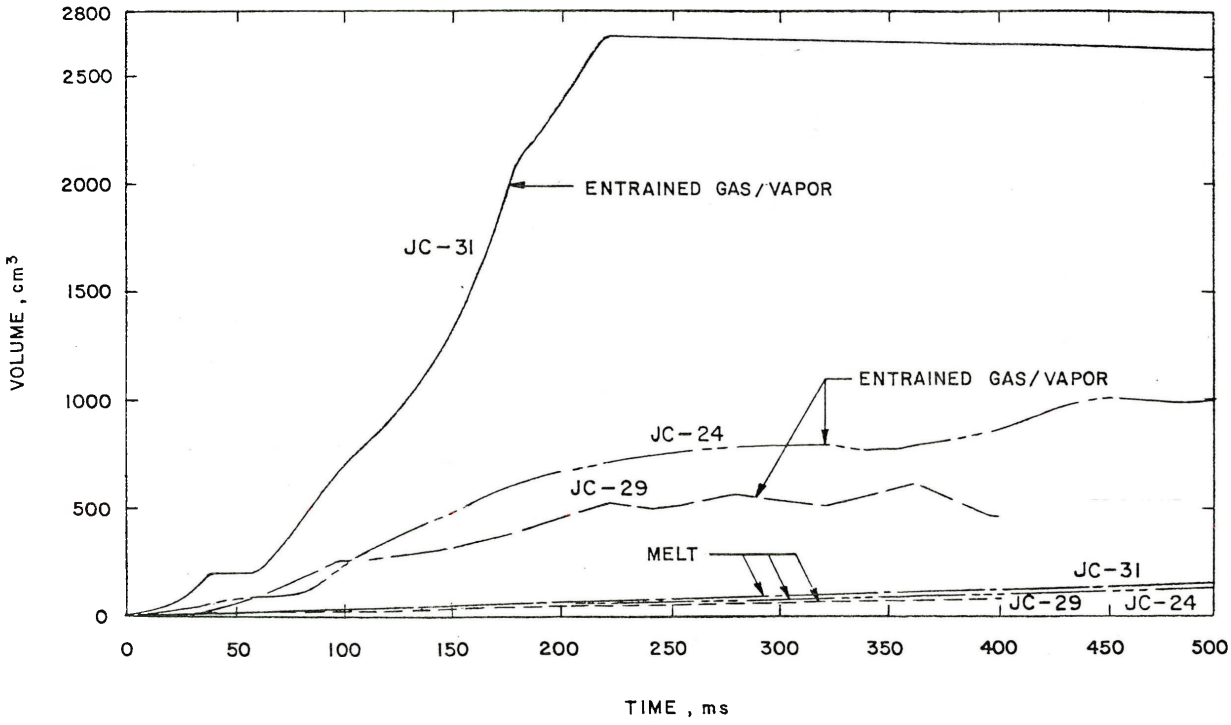

Figure 37. Pool Swell for JC-24, -29, and -31.

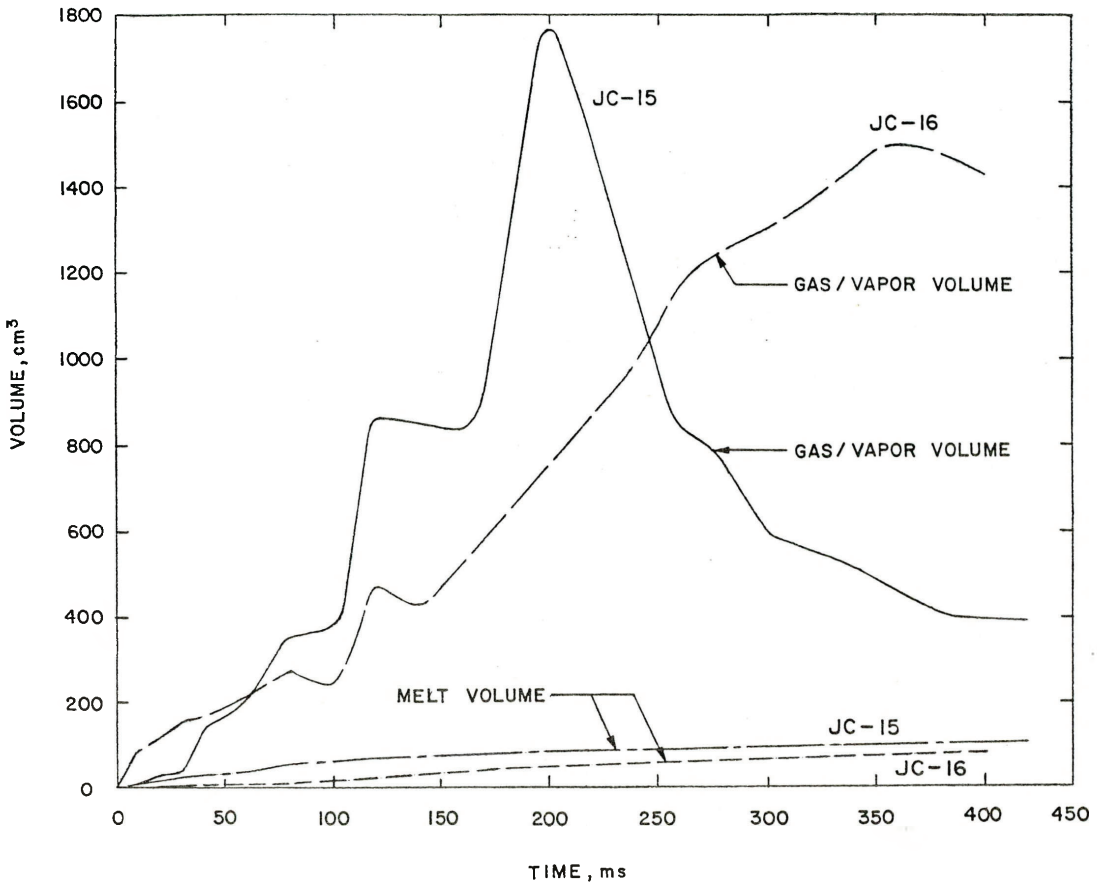

Figure 38. Pool Swell for JC-15 and -16

TABLE IV. Estimated Void Fractions of the Mixing Zone

Position of Leading Edge below Initial Water Level, mm	Void Fraction JC-24	JC-31
51	0.44	0.93
152	0.25	0.88
305	0.26	0.84

boiling, the void fraction of the mixing zone for JC-24 is less than that for JC-31 because the mixing zone was defined as the region observed to consist of vapor bubbles, pour stream, drops, and frozen particles.

The same behavior occurred in test FFC-8 involving U - 5 w/o Zr alloy pressurized with argon to 880 KPa and injected into sodium at 600C as in JC-3 and -5.[23] In that test the sodium temperature was monitored and a rapid decline in sodium temperature was observed indicating a large gas flow displacing the sodium in spite of the injection of a melt at a higher temperature of 1624C (see Fig. 39). In previous experiments with a gravity drop the thermocouples indicated temperature increases during injection.

The apparatus for the uranium metal alloy drops in sodium was similar in concept to that shown in Fig. 2 for the low melting point metals in water. The uranium alloy was melted by induction heating in a MgO crucible. The stainless steel interaction vessel which contained the sodium was 192 mm in internal diameter. The sodium depth was 1.22 m for these tests. The test vessel was contained within a 0.457-m diameter pressure vessel, and the entire assembly was located in a concrete cell. A detailed description of the apparatus and the experiments is given in the report by Gabor et al.[23]

6. Breakup Model Evaluation

It is obvious from the complexity of the breakup mechanisms observed in these tests that a simple model based on first principles would not

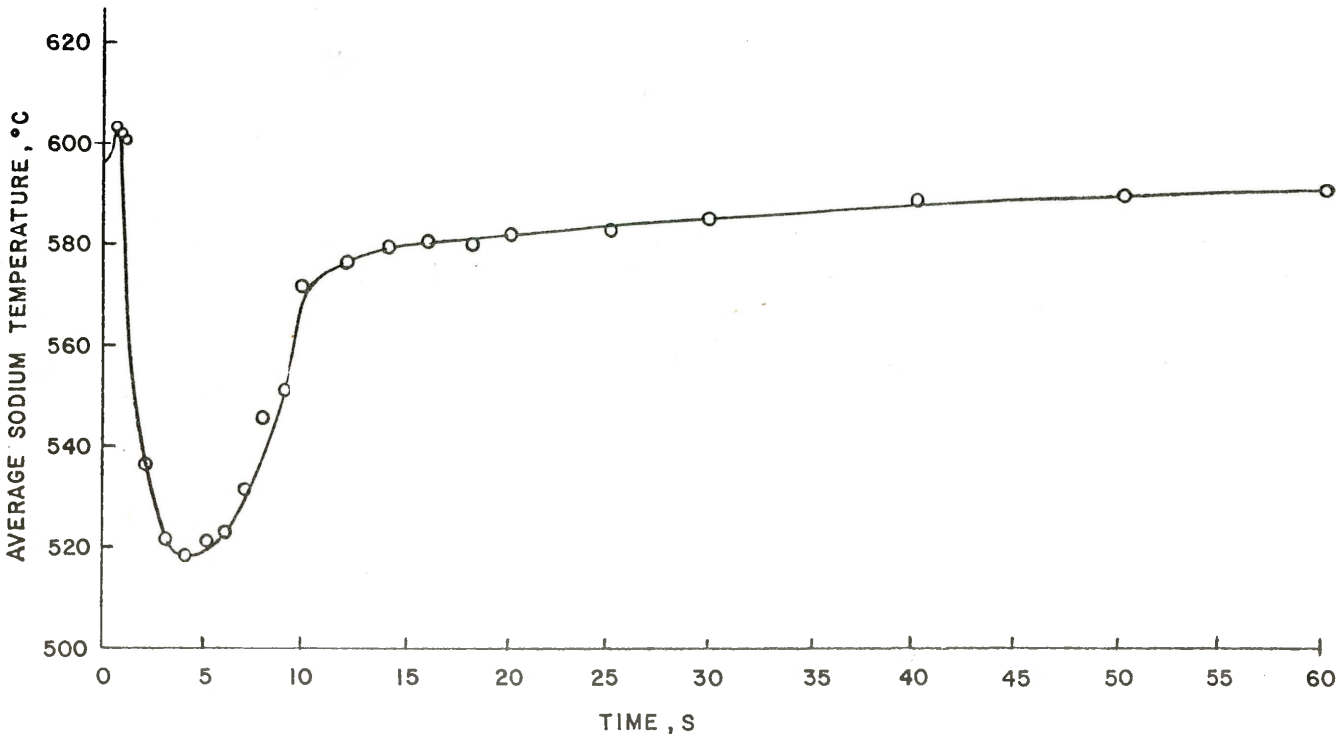

Figure 39. Sodium Temperature Response to FFC-8 Pressurized Injection[23]

describe all aspects of the breakup phenomena. However, a comparison of these experimental results with the breakup length correlations discussed in Section I is helpful in reactor safety assessments. Calculated jet breakup distances for the various correlations or models are listed in Table V. For the most part, the predicted breakup lengths differ significantly from those observed in these tests (Section II.E.4) as would be expected from the idealized bases for these correlations and models. These correlations and models were for small diameter jets injected into a single phase media. The Taylor[12] and Epstein and Fauske[16] models gave reasonable predictions for the conditions of these tests.

TABLE V. Calculated Pour Stream Breakup Ratios for Wood's Metal

D_{ji} = 0.025 m			U_o = 2 m/s
Correlation or Model	Equation No.	Breakup Ratio L/D_{ji}	Comments
Rayleigh-Levich	(3)	144	Steam environment
Weber	(4)	600	Steam environment
Taylor	(5)	660	Steam environment
		16	Water environment
Baron	(6)	10	Turbulent regime
Epstein-Fauske	(7)	108	Steam blanket
Epstein-Fauske	(8)	3	Water
Levich	(9)	0.02	Sinuous wave in steam
Levich	(10)	7,700	High-velocity jet in steam
Levich	(11)	8,560	Viscous jet in steam
Grant-Middleman	(12)	520	Steam environment
Grant-Middleman	(13)	100	Turbulent jet in steam
Phinney	(14)	107	Turbulent jet

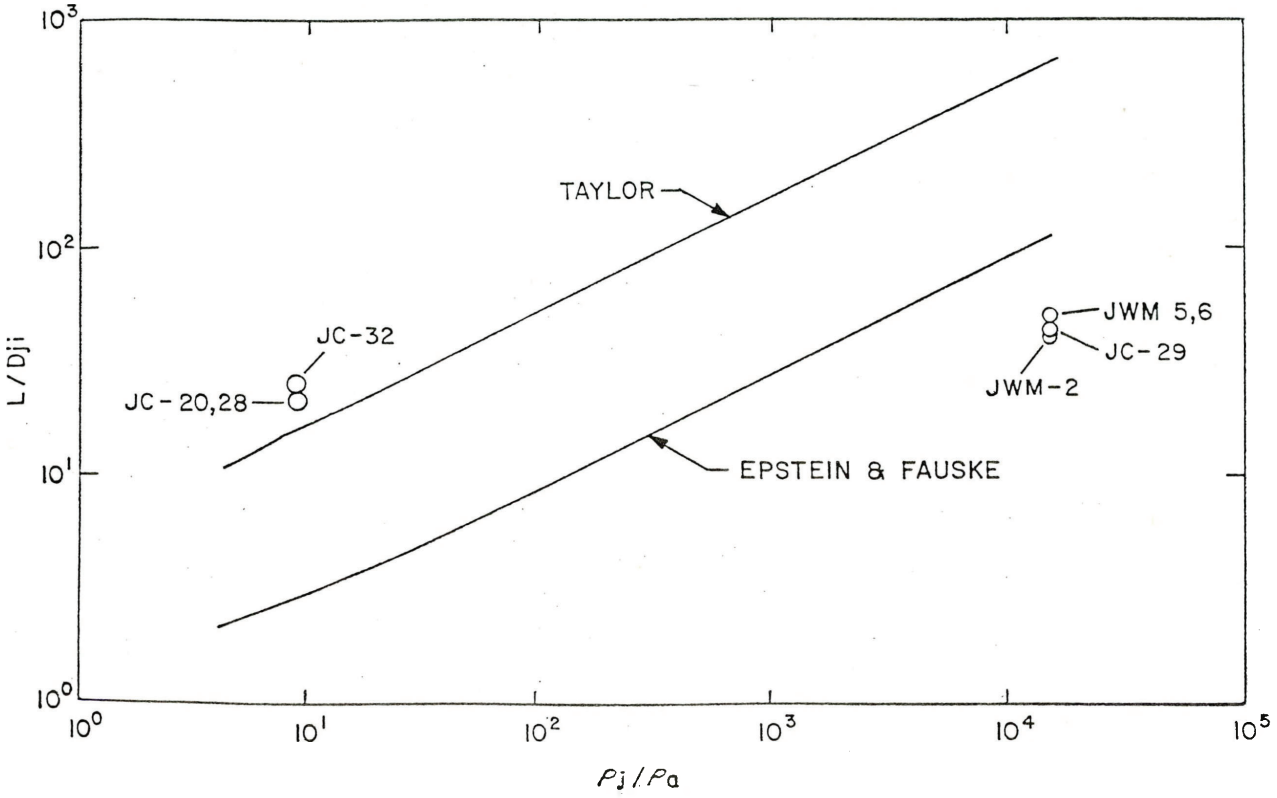

Figure 40. Comparison of Observed Breakup Lengths with Models by Taylor and Epstein and Fauske

The observed breakup distances normalized in terms of the entrance jet diameter versus the ratio of the jet density to the ambient fluid density, ρ_j/ρ_a, are compared with the Taylor semi-empirical model and the Epstein and Fauske model on Fig. 40. The ambient fluid was assumed to be water for those tests performed with subcooled water and steam for tests with saturated water resulting in steam generation. The latter assumption is highly in question. A two-phase ambient fluid density would most likely be more correct. The measured L/D_{ji} of approximately 20 to 25 for jet breakup in water is in reasonable agreement with the Taylor model. The data agreed better with the Epstein and Fauske model in the vapor-dominated regime when the density of steam for ρ_a is used.

Also shown on Fig. 40 are data for tests with Cerrotru pour streams. The pour stream temperatures were 250, 450, and 400C for tests JWM-2, 5, and 6, respectively, and the water temperature was at 100C. The breakup lengths were based on change in the pour stream penetration rate and observation from the motion pictures. Because the Cerrotru melting point is at 138C, the melt material solidified in the 100C water whereas they did not in the Wood's metal test JC-29. The L/D_{ji} ratio of about 40 to 50 was determined for cases where steam was generated by the pour stream in water at 100C. If a two-phase fluid density for the ambient density rather than steam density were used so that ρ_j/ρ_a is 100, then these data would agree with the Taylor model. A value of $\rho_j/\rho_a = 2500$ would give agreement with the Epstein and Fauske model.

III. CONCLUSIONS

1. It appears possible to characterize the breakup length of a pour stream in water by change in leading edge penetration rate.

2. Entrainment and heat transfer from the leading edge vortex ball dominated the initial penetration stage.

3. In tests without net steam generation, the pour stream breakup length measured 20 to 25 L/D_{ji}.

4. Tests with steam generation (water at 100C) resulted in greater breakup lengths of about 40 to 50 L/D_{ji}.

5. The characteristics of the particles produced by the pour stream breakup were dependent on the test conditions. Flake-like particles were formed by freezing of the pour stream surface and separation from the flowing molten core. Filaments and globules resulted from surface tension forces. The high-velocity pour stream resulted in finer fragmentation, whereas increasing melt temperature had little effect on the overall size distribution.

6. The size of the mixing zone which included metal fragments, vapor/gas, and pour stream core was a function of the melt and water temperature which determined the vapor generation rate.

7. The measured L/D_{ji} for pour stream breakup in water was in reasonable agreement with the Taylor model.

8. The data for tests with steam generation agreed better with the Epstein and Fauske model when the density of steam was used for the ambient fluid.

9. A Wood's metal pour stream in air maintained its integrity with no tendency for breakup during the entire length (2 m or $L/D_{ji} = 40$) of visible drop.

10. Increasing the argon gas pressure in the furnace/injector did increase the velocity of the melt flow but resulted in a two-phase behavior which was not comparable with the other tests with a single-phase pour stream flow.

11. While entrainment of noncondensable air above the water pool was large as the pour stream entered the pool, it had little effect on the penetration rate and subsequent breakup.

IV. ACKNOWLEDGMENTS

This experimental study is the result of the cooperation and contributions of a number of individuals. The efficient and timely processing of this report by V. Eustace is greatly appreciated. Much thanks are owed to T. M. George, a co-op student from the University of Cincinnati, for his film analysis and assistance in the experimental operations. The assistance of B. T. Banez with the instrumentation and data reduction is gratefully acknowledged. The help of D. J. Kilsdonk and W. H. Gunther in many vital ways is duly noted with appreciation. J. Kawka prepared the figures for this report for which we are grateful.

V. REFERENCES

1. T. Ginsberg, "Liquid Jet Breakup Characterization with Application to Melt-Water Mixing," ANS Proc, 1985 Natl Heat Transfer Conf, ANS #700101, Denver, CO (August 1986).

2. M. J. McCarthy and N. A. Malloy, "Review of Stability of Liquid Jets and the Influence of Nozzle Design," The Chemical Engineering Journal, 7, pp. 1-20 (1974).

3. Y. Kitamura and T. Takahashi, "Stability of Jets in Liquid-Liquid Systems," Encyclopedia of Fluid Mechanics, Vol. 2, Gulf Publishing Co., Houston, TX (1986).

4. R. D. Reitz, "Atomization and Other Breakup Regimes in a Liquid Jet," PhD Dissertation, Princeton Univ., Dept. Mechanical and Aerospace Eng. (October 1978).

5. B. W. Spencer, L. McUmber, D. Gregorash, R. Aeschlimann, and J. Sienicki, "Corium Quench in Deep Pool Mixing Experiments," ANS Proc, 1985 Natl Heat Transfer Conf, ANS #700101, Denver, CO (August 1985).

6. J. W. S. Rayleigh, "The Theory of Sound," Dover Publications, New York, NY (1945).

7. V. C. Levich, "Physiochemical Hydrodynamics," Prentice-Hall, Inc., Englewood Cliffs, NJ (1962).

8. C. Weber, "On the Breakdown of a Fluid Jet," Z. Angew. Math. Mech., 11, p. 136 (1931).

9. W. E. Ranz, "Some Experiments on Orifice Sprays," Can. J. Chem. Eng., pp. 175-181 (August, 1958).

10. A. M. Sterling and C. A. Sleicher, "The Destability of Capillary Jets," J. Fluid Mech., 68, p. 477 (1975).

11. G. I. Taylor, "Generation of Ripples by Wind Blowing Over a Viscous Fluid," The Scientific Papers of G. I. Taylor, Vol. III, ed. G. K. Batchelor (1940).

12. G. I. Taylor, "The Dispersion of Jets of Metals at Low Melting Point in Water," The Scientific Papers of G. I. Taylor, Vol. III, ed. G. K. Batchelor (1940).

13. T. Baron, Technical Report, University of Illinois, No. 4 (1949).

14. G. Littaye, "Sur une Theorie de la Pulverisation des Jets Liquides," Compt. Read., 217, p. 99 (1943).

15. S. W. J. Smith and H. Moss, "Experiments with Mercury Jets," Proc. Roy. Soc. London, 93, p. 373 (1917).

16. M. Epstein and H. K. Fauske, "Steam Film Instability and the Mixing of Core-melt Jets and Water," ANS Proc, 1985 Natl Heat Transfer Conf, ANS #700101, Denver, CO (August 1985).

17. R. P. Grant and S. Middleman, "Newtonian Jet Stability," AIChE Journal, 12, p. 569 (1966).

18. R. E. Phinney, "The Stability of High-speed Viscous Jets: The Effect of an Ambient Gas," Phys. Fluids, 16, p. 123 (1973).

19. K. Hartel, "A Linear Model for the Determination of Hydrodynamic Stability of Liquid Jets in Liquids," KFK 3978, Karlsruhe, ed. K. Marten (1985).

20. K. Marten, V. Casal, and K. J. Mack, "Model Experiments to Study the Stability of a Fuel Jet in Sodium," KFK 3989, Karlsruhe (1985).

21. B. W. Spencer, J. D. Gabor, J. C. Cassulo, and D. J. Kilsdonk, "Results of Scoping Experiments on Melt Stream Breakup and Quench," Proc Intl ANS/ENS Topical Mtg on Thermal Reactor Safety, ANS #700106, San Diego, CA (February 2-6, 1986).

22. B. W. Spencer, J. D. Gabor, and J. C. Cassulo, "Effect of Boiling Regime on Melt Stream Breakup in Water," Fourth International Symposium on Multi-phase Transport and Particulate Phenomena, Miami Beach (December 15-17, 1986).

23. J. D. Gabor, R. T. Purviance, R. W. Aeschlimann, and B. W. Spencer, "Characterization of Metal Fuel Fragmentation," ANL-IFR-52, Argonne National Lab. (1986).

24. A. J. Reynolds, "Observations of a Liquid-into-liquid Jet," J. Fluid Mech, 14, pp. 552-556 (1962).

25. D. F. Hopkins and J. M. Robertson, "Two-dimensional Incompressible Fluid Jet Penetration," J. Fluid Mech, 29, part 2, pp. 273-287 (1967).

26. B. W. Marshall, Jr. and M. Berman, "An Experimental Study of Isothermal and Boiling Liquid Jets," 14th Water Reactor Safety Research Information Meeting, Gaithersburg, ML (October 27-31, 1986).

27. K. J. McNaughton and C. G. Sinclair, "Submerged Jets in Short Cylindrical Flow Vessels," J. Fluid Mech, 25, Part 2, pp. 367-375 (1966).

28. J. F. Richardson and W. N. Zaki, "Sedimentation and Fluidisation, Part I," Trans. Instn. Chem. Engrs, Lond., 32, p. 35 (1961).

29. J. H. Perry, Ed., "Chemical Engineers' Handbook," Third Ed., McGraw-Hill Book Co., New York, NY (1950).

30. C. M. Adams, Jr., "Thermal Considerations in Freezing," Liquid Metals and Solidification, Amer. Society of Metals, pp. 187-217 (1958).

31. W. H. McAdams, "Heat Transmission," McGraw-Hill Book Co., NY (1954).

32. F. B. Cheung and L. Baker, Jr., "Postaccident Heat Removal: Transient Freezing of Liquids in Tube Flow," ANL/RAS 75-41 (October 1975).

33. J. Iciek, V. Cywinska, and R. Blaszczyk, "Hydrodynamics of Free-liquid Jets and Their Influence on Heat Transfer," Handbook of Heat and Mass Transfer Vol. 1: Heat Transfer Operations, N. P. Cheremisinoff, Ed., Gulf Publishing Co., Houston, TX (1986).

34. V. Gat and R. A. Green, "Direct Contact Heat Transfer from an Immiscible Liquid Jet," Warme und Stoffübertragung, 9, pp. 13-20 (1976).

35. V. T. Morgan, "The Overall Convective Heat Transfer from Smooth Circular Cylinders," Advances in Heat Transfer, Vol. 11, Academic Press, NY, pp. 199-264 (1975).

36. R. N. Lyon, Chem. Eng. Progr., 47, pp. 75-79 (1951).

37. L. A. Bromley, Chem. Eng. Progr., 16, p. 221 (1950).

38. K. J. Baumeister, F. F. Simon, and R. E. Henry, ASME Symp., "Augmentation of Convective Heat Mass Transfer," ASME Winter Annual Meeting, New York (1970).

39. P. J. Berenson, "Film-boiling Heat Transfer from a Horizontal Surface," J. of Heat Transfer, 83, pp. 351-8 (1961).

40. R. E. Henry, "A Correlation for the Minimum Film Boiling Temperature," AIChE Symp. Series No. 138, 70, pp. 81-90 (1974).

41. M. T. Farmer and B. W. Spencer, "Effects of Water Subcooling, Purity, and Pool Agitation on the Minimum Film Boiling Temperature for Metal and Oxide Surfaces," ANL/LWR/SAF 84-2 (1984).

42. Y. Kikuchi, T. Hori, and I. Michiyoshi, "Minimum Film Boiling Temperature for Cooldown of Insulated Metals in Saturated Liquid," Int. J. Heat Mass Transfer, 28, pp. 1105-1114 (1985).

43. P. Spiegler, J. Hopenfeld, M. Silberberg, C. F. Bumpus Jr., and A. Norman, "Onset of Stable Film Boiling and the Foam Limit," Int. J. Heat Mass Transfer, 6, pp. 987-989 (1963).

APPENDICES

Appendix A

Settling Velocity

The settling velocity, V, for an interacting swarm of particles has been related to the terminal velocity, V_∞, for a single particle in an infinite medium by Richardson and Zaki[28] by:

$$v = V_\infty \varepsilon^n \tag{A1}$$

where ε is the voidage or the liquid fraction, and n is 2.34 for particle Reynolds numbers greater than 500.

The terminal velocity is related to the drag coefficient, C, by:

$$V_\infty = \sqrt{\frac{2gm(\rho_s - \rho_f)}{\rho_f \rho_s A_p C}} \tag{A2}$$

where m is the particle mass, A_p the area of the particle projected on the plane normal to the direction of motion, ρ_s the particle density, and ρ_f the fluid density. The drag coefficient is related to the particle Reynolds number in Perry[29] for spherical, cylindrical, and disk shaped particles.

Equation A1 shows that as the void fraction decreases the settling velocity also decreases. This can be used in interpreting the velocity changes of the pour stream leading edge. Initially before pour stream breakup the voidage is high and therefore the velocity is high. At breakup a swarm of particles with reduced voidage settles at a reduced velocity. As the mixing zone expands the voidage increases with a subsequent velocity increase.

Appendix B

Solidification Times of Molten Metal Pour Streams in Liquid Coolant

The quench mechanism of molten metal pour streams in liquid coolant is dependent on the extent of solidification of the stream material during hydrodynamic breakup. Several solidification models are discussed below. These models 1) estimate solidification time for a limiting case of no breakup and 2) give an order of magnitude comparison between the leading edge heat flux and trailing column heat flux. It is recognized that these models are not applicable during hydrodynamic breakup.

Model 1 - Negligible Heat Capacity of Solid Phase

If the pour stream is treated as a mass of internally nonflowing liquid moving through the coolant phase, solidification of a cylindrical body can be a limiting case basis for modeling. An exact solution can be obtained by assuming that the heat capacity of the solid phase is negligible relative to the latent heat of solidification, λ, and that the liquid temperature is at the freezing temperature, T_f. In reference to the conditions indicated on Fig. B1, the following boundary conditions are given.

$$\text{at } r = r_o \qquad -K_s \frac{\partial T}{\partial r} = h\,(T_f - T_c)$$

$$\text{at } r = r_o - \varepsilon \qquad -K_s \frac{\partial T}{\partial r} + K_\ell \frac{\partial T}{\partial r} = \rho_s \lambda \frac{dr}{dt}$$

where

h = jet-to-coolant heat transfer coefficient,

T_c = liquid coolant temperature,

K_s = solid phase thermal conductivity for pour stream,

K_ℓ = liquid phase thermal conductivity for pour stream,

ρ_s = density of solid phase,

t = time,

ε = thickness of solidified zone.

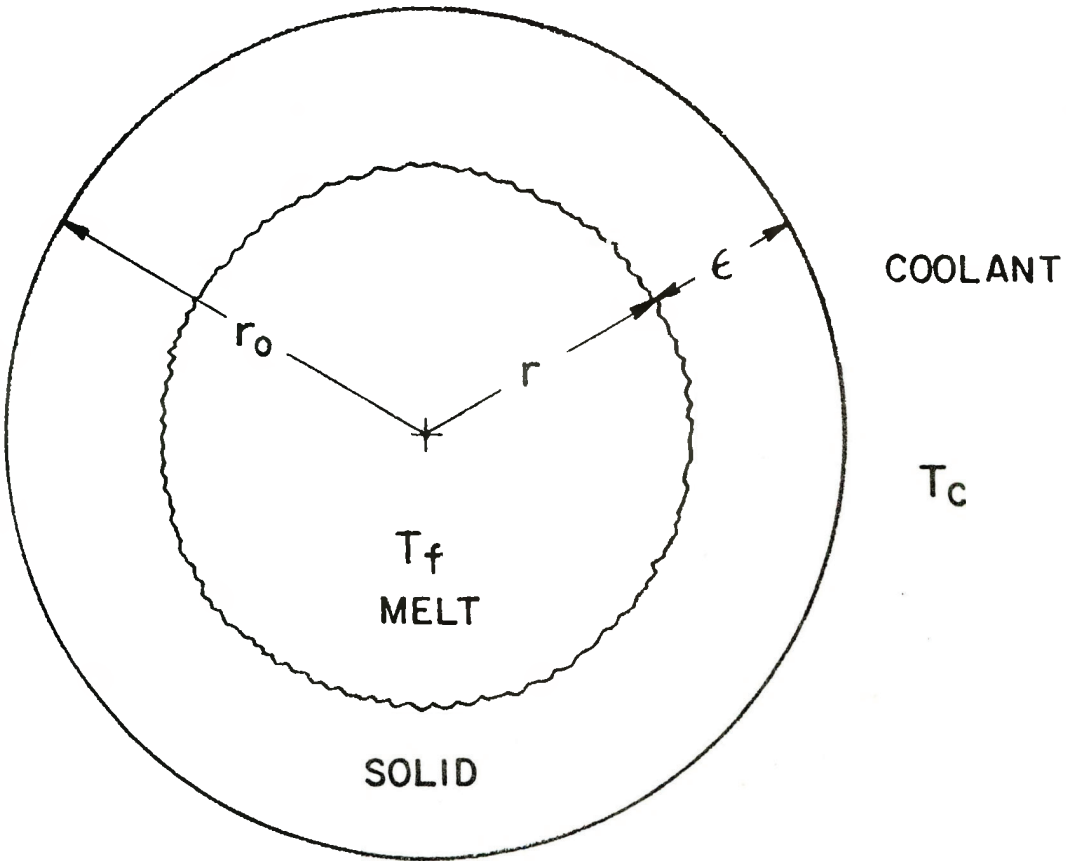

Figure B1. Melt Front in Cylindrical Body

The heat flux, q, relative to the external surface area of the pour stream is:

$$q = \frac{(T_f - T_c)\, 2\pi L}{\frac{1}{hr_o} + \frac{\ln \frac{r_o}{r_o - \epsilon}}{K_s}} \tag{B1}$$

where L is the pour stream length.

The heat flux can be related to the melt front by:

$$q = \rho\lambda 2\pi L\, (r_o - \epsilon)\, \frac{d\epsilon}{dt} \tag{B2}$$

Let

$$Bi = \frac{hr_o}{K}\,,\quad R = \frac{r_o - \epsilon}{r_o}\,,\quad \text{and}\quad \theta = \frac{h^2}{\rho\lambda K_s}\,(T_f - T_c)\, t$$

which leads to:

$$\frac{(T_f - T_c)\, 2\pi L K_s}{\frac{1}{Bi} - \ln R} = -\,\rho\lambda 2\pi L\, r_o^{\,2}\, R\, \frac{dR}{dt} \tag{B3}$$

$$\frac{K_s}{\rho\lambda r_o^{\,2}}\,(T_f - T_c)\, dt = -\left(\frac{1}{Bi} - \ln R\right) R\, dR$$

Integration gives

$$\frac{K_s}{\rho\lambda r_o}\,(T_f - T_c)\, t = \frac{R^2}{2}\left[-\left(\frac{1}{Bi} + \ln R - \frac{1}{4}\right)\right]_1^R$$

or

$$\theta = \frac{B_i^{\,2}}{2}\left[\left(\frac{1}{Bi} + \frac{1}{2}\right)\left(1 - R^2\right) + R^2 \ln R\right] \tag{B4}$$

Complete solidification occurs when R=0 which results in:

$$\theta = \frac{Bi^2}{2}\left(\frac{1}{Bi} + \frac{1}{2}\right) \qquad \text{for } R = 0 \tag{B5}$$

Model 2 - Negligible Pour Stream-to-Coolant Resistance

The partial difference equation for heat flow in cylindrical coordinates is

$$\frac{\partial T}{\partial t} = \frac{K_s}{\rho_s C_{P_s}}\left[\frac{\partial^2 T}{\partial r^2} + \frac{1}{r}\frac{\partial T}{\partial t}\right] \tag{B6}$$

The above equation takes into account the heat capacity, C_{P_s}, of the solid phase. Assuming the melt phase to be initially at the freezing temperature and the wall temperature at the coolant temperature (negligible pour stream-to-coolant resistance) Adams[30] numerical integration obtained the time for complete solidification. Adams's solution is plotted in Fig. B2.

Model 3 - Inclusion of Superheat

Adams[30] suggests an estimation for the time for superheat removal by calculating the time required for the center temperature to decrease 50% with the surface temperature at time 0 suddenly reduced to T_f. A better estimation can be achieved by solving Eq. B6 numerically for both the solid and liquid phases. This can be achieved by transposing cylindrical coordinates to linear coordinates by letting

$$\beta = \ln r$$

then

$$\frac{\partial T}{\partial t} = \frac{K_s}{\rho_s C_{Ps}}\left[\frac{\partial^2 T}{\partial r^2} + \frac{1}{r}\frac{\partial T}{\partial r}\right] = \frac{K_s}{\rho_s C_{Ps}}\frac{\partial^2 T}{\partial \beta^2} \tag{B7}$$

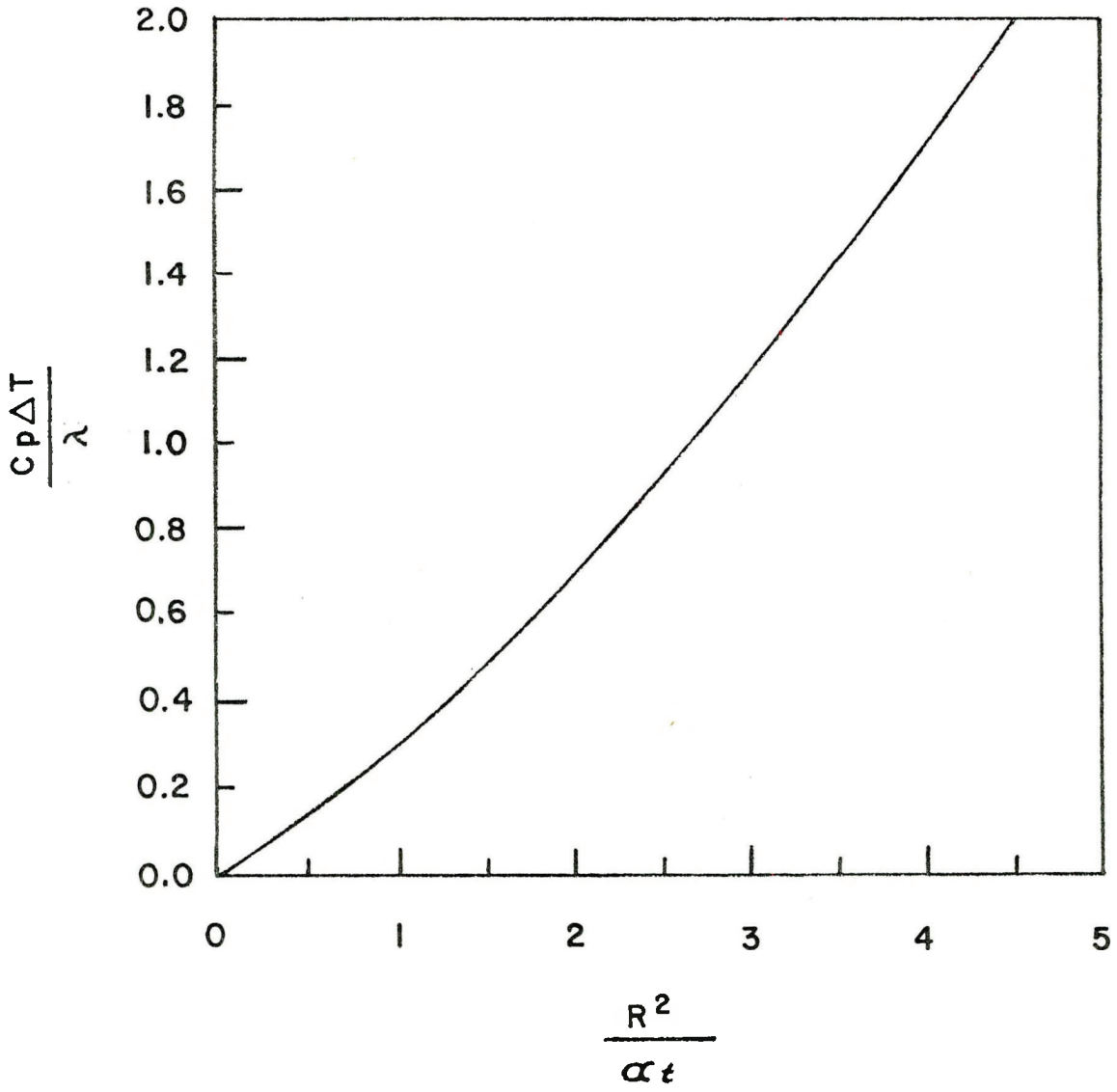

Figure B2. Times for Complete Solidification of Cylinders

and

$$\frac{\partial T}{\partial t} = \frac{K_{\ell}}{\rho_{\ell} C_{P\ell}} \frac{\partial^2 T}{\partial \beta^2} \tag{B8}$$

For numerical analysis, incremental terms are used yielding:

$$\frac{\Delta T}{\Delta t} = \frac{K_s}{\rho_s C_{Ps}} \frac{1}{\Delta \beta^2} \Delta^2 T \tag{B9}$$

or

$$T_{n,m+1} - T_{n,m} = \frac{K_s}{\rho_s C_{Ps}} \frac{\Delta t}{\Delta \beta^2} \left[\left(T_{n+1,m} - T_{n,m} \right) - \left(T_{n,m} - T_{n-1,m} \right) \right] \tag{B10}$$

where n refers to position and m to time increments.

If $\frac{K_s}{\rho_s C_{Ps}} \frac{\Delta t}{\Delta \beta^2}$ is set equal to $\frac{1}{2}$, then

$$T_{n,m+1} = \frac{1}{2} \left(T_{n+1,m} + T_{n-1,m} \right)$$

This relation is the basis for the Schmidt numerical method[31] and facilitates solution for both the solid and liquid phases of the pour stream with adjustment for the progressing melt interface and inclusion of pour stream-to-coolant resistance.

Model 4 - Flowing Fluid

Another model would be to visualize the pour stream as a stream flowing through a tube rather than as a cylinder of molten material in plug flow. For this model the empirical correlation of Cheung and Baker[32] can be used:

$$\frac{Z}{D} \left(\frac{\alpha_s}{\alpha_{\ell}} \right)^{1/9} Re^{-3/4} \left[\frac{C_{ps} (T_f - T_w)}{\lambda} \right]^{1/3} \left[1 + 0.7 \frac{C_{P\ell} (T_o - T_f)}{\lambda} \right]^{-1} = 0.23 \, Pr^{1/2} \tag{B12}$$

where

Z = distance which melt can flow before plugging,
D = tube diameter,
Re = Reynolds number,
Pr = Prandtl number.

This model which includes superheat is for a fixed wall confining the molten material and not a free liquid-liquid interface. If the velocity is assumed constant until freezing occurs, the time for freezing can be determined from the distance the melt flows before plugging. This is not reflective of complete solidification however.

Determination of Coolant-to-Pour Stream Heat Transfer Coefficient

Liquid-to-Pour Stream Contact

Surprisingly there is a scarcity of data for heat transfer from a liquid external to a single cylinder flowing in the direction of the cylinder axis and for jet-to-liquid heat transfer. Iciek et al.[33] reported steam condensation on jets of cold water and Gat and Green[34] obtained data but did not present a general correlation for a laminar jet flowing around a coaxial wire. The wire served as a thermocouple probe and also altered the jet velocity profile. For these calculations heat transfer coefficients will be estimated from correlations for fluid flow parallel to a cylinder. Morgan[35] suggests that the heat transfer coefficient is 40% of that for fluid flow normal to a cylinder. Then:

$$h = \left(\frac{K_f}{D}\right)\left[0.42\ Pr^{0.2} + 0.57\ Pr^{0.33}\ Re^{0.5}\right](0.4) \qquad \text{(B13)}$$

The heat transfer coefficient can also be estimated if the radius of curvature is neglected. The average heat transfer coefficient over a flat plate of length L is:

$$h = \left(\frac{2}{3}\right)\left(\frac{K_f}{L}\right)\left(\frac{LV\rho_f}{\mu_f}\right)^{1/2} P_r^{1/3} \qquad \text{(B14)}$$

Another consideration is that of annular flow since the container diameter to pour stream diameter is about 8 to 1 for most of the simulant material and reactor material tests. For turbulent vertical flow in a concentric annulus, the following equation was used[31]:

$$h = \frac{k}{D_e} (0.023) (Re)^{.8} (Pr)^{.33} (\Psi) \qquad \text{(B15)}$$

where

$$D_e = \frac{D_{out}^2 - D_{in}^2}{D_{out} + D_{in}}$$

$$\Psi = \left(\frac{D_{out}}{D_{in}}\right)^{0.45}$$

Lyon[36] proposed the following equation for liquid metal heat transfer in a concentric double-pipe heat exchanger:

$$h = \frac{K}{D_e} \left(4.9 + 0.0175\ Re^{0.8}\right) \qquad \text{(B16)}$$

Equations B13-B16 give heat transfer coefficients for liquids with zero voidage at the heat transfer surface.

Vapor-to-Pour Stream Contact

The least favorable case for heat transfer is to assume that the pour stream is completely surrounded by vapor. Equations B13-B15 can be used with the vapor properties for the fluid phase.

Film Boiling on Pour Stream Surface

An intermediate case between 100 percent liquid and 100 percent vapor contact is film boiling on the pour stream surface. Bromley[37] suggested the following equation for a vertical tube:

$$h = 0.7 \left[\frac{K_v^3 \rho_v (\rho_\ell - \rho_v) g (h_{\ell v} + 0.4 C_{pv} \Delta T)}{L \mu_v (T_w - T_{sat})} \right]^{1/4} \quad \text{(B17)}$$

where

L = tube length,

$h_{\ell v}$ = heat of vaporization.

Discussion of Results

Consideration was given to tin and Wood's metal dropped into water and U - 5 w/o Zr in sodium. Heat transfer coefficients from melt to coolant are estimated using the various correlations for a pour stream diameter of 25 mm, length of 0.305 m, and velocity of 2 m/s (see Table B-I). For annular flow with the liquid coolant container diameter 8 times as large as the pour stream diameter, D_e is 0.178 m. Calculations of solidification times were based on the heat transfer coefficient determined from Eq. B13. This equation was thought to be most physically appropriate. The solidification times were calculated for Models 1 and 2 for the pour stream surrounded by liquid with no vapor voidage, surrounded entirely by vapor, and partially surrounded by liquid (film boiling).

The results of the calculations for solidification times are listed in Table B-II. In all cases the time for complete solidification requires at least a second. This indicates that hydrodynamic processes are in effect during the quench process. It would be expected that the extent of fragmentation would be inversely related to the solidification time unless, of course, the melt does not solidify until after it contacts the bottom of the coolant pool. The solidification times determined from Model 4 include the effect of superheat but are not the times required for complete solidification. The times were calculated from the length the melt would flow in a 25 mm diameter tube before plugging with a flow velocity of 2 m/s.

This examination suggests hydrodynamic breakup of the pour streams in these tests is initiated before solidification of the pour stream occurs.

TABLE B-I. Jet-to-Coolant Heat Transfer Coefficients

		$h, w/m^2 \cdot K$				
Coolant	T,K	Eq. B13	Eq. B14	Eq. B15	Eq. B16	Eq. B17
Water (ℓ)	298.2	2365	1987	10,955		
Water (ℓ)	373.2	3079	2577	19,805		
Water (v)	373.2	11.4	9.4	20.3		100
Sodium (ℓ)	873.2	41,318	33,831	271,494	505,000	
Sodium (v)	1154.6	14.7	12.0	17.6		

TABLE B-II. Solidification Times

Melt Material	Ambient Fluid	$h, w/m^2 \cdot K$	Time, s		
			Model 1	Model 2	Model 4
Wood's metal (346 K)	Water (298 K)	2365	49.7	29.5	
Wood's metal (375 K)	Water (298 K)				10.6
Tin (505K)	Water (298 K)	2365	6.6	1.8	
Tin (605 K)	Water (298 K)				3.1
Tin (505 K)	Water (372 K)	3079	8.4	2.6	
Tin (505 K)	Water vapor (372 K)	11.4	1717	2.6	
Tin (505 K)	Water film boiling	100	198		
U - 5 w/o Zr (1524 K)	Sodium (873 K)	41,318	1.3	1.9	
U - 5 w/o Zr (1624 K)	Sodium (873 K)				3.6
U - 5 w/o Zr (1524 K)	Sodium vapor (1155 K)	14.7	1095	2.9	

Appendix C

Calculation of Film Boiling of Water on Wood's Metal Surface

These calculations were performed in preparation for test JC-24 in order to obtain an indication of the Wood's metal temperature required for film boiling. The experiment was conducted under the maximum capability of the apparatus which permitted a melt temperature of 445C.

The minimum film-boiling heat flux for steady-state heat transfer from a horizontal surface was experimentally determined to occur at a surface-water ΔT_{min} of 135K.[38] Berenson[39] assuming Taylor-Helmhotz hydrodynamic instability developed the following equation for ΔT_{min}:

$$\Delta T_{min} = 0.127 \frac{\rho_v h_{\ell v}}{k_v} \left[\frac{g(\rho_\ell - \rho_v)}{\rho_\ell + \rho_v}\right]^{\frac{2}{3}} \left[\frac{\sigma}{g(\rho_\ell - \rho_v)}\right]^{\frac{1}{2}} \left[\frac{\mu_v}{g(\rho_\ell - \rho_v)}\right]^{\frac{1}{3}} \qquad (C1)$$

ΔT_{min} was calculated using properties of Table C-I. This calculation is compared with those of Henry[40] and Farmer[41] (see Table C-I).

The interaction between the Wood's metal jet and the water is a transient event and consideration should be given to the temperature gradient near the metal surface. Henry[40] presented a correlation which takes into account the interface temperature:

$$\frac{T'_{min} - (T'_{min})_I}{(T'_{min})_I - T_\ell} = 0.42 \left[\sqrt{\frac{K_\ell \rho_\ell C_\ell}{K_w \rho_w C_w}} \frac{h_{\ell v}}{(\Delta T_{min})_I}\right]^{0.6} \qquad (C2)$$

The bulk Wood's metal temperature, T'_{min}, (Table C-I) was calculated using the various $\Delta T_{min's}$ from Table C-I. The experimental work by Farmer indicates that minimum film boiling occurs somewhere between the temperature predicted by Berenson's equation and that prediction from Henry's correlation. Experimental work by Kikuchi et al.[42] on transient cooling of copper plates in

TABLE C-I. Calculated Wood's Metal Bulk Temperature Required for Film Boiling

ΔT_{min} Calculation	ΔT_{min}, °C	T'_{min}, °C
Henry	75.6	556
Farmer	60.0	506
Authors	85.7	585

liquid nitrogen resulted in minimum film boiling temperatures between that predicted by Spiegler et al.[43] $\left(T_{min} = \frac{27}{32} T_{crit}\right)$ and that predicted by Berenson[34] (Eq. C1). Also to be noted is that the interface temperature between Wood's metal at 585C and liquid water at 100C is calculated to be 456C, which is greater than the homogeneous nucleation temperature of water (305C).

Nomenclature

C = specific heat

g = acceleration of gravity

$h_{\ell v}$ = latent heat of vaporization

k = thermal conductivity

T_{crit} = critical temperature

T_{ℓ} = liquid bulk temperature

T'_{min} = metal melt bulk temperature at minimum film boiling temperature

$(T'_{min})_I = (\Delta T_{min})_I + T_{sat}$

ΔT_{min} = temperature difference between surface temperature and T_{sat}

$(\Delta T_{min})_I$ = ΔT_{min} calculated by Berenson's calculation

T_{sat} = saturation temperature of liquid phase

Greek letters

Δ = difference

μ = viscosity

ρ = density

σ = surface tension

Subscripts

I = isothermal

ℓ = liquid

min = minimum film boiling point

sat = saturation

v = vapor

w = wall

Appendix D

Model for Breakup Distance Based on Balance of Drag Force and Surface Tension Force

Although the initial velocity of the pour stream is low (2 m/s), the large diameter and high density of the Wood's metal places the jet Reynolds number well into the turbulent regime. This, therefore, puts into question the application of the classical theories based on potential flow. It was observed in the Wood's metal drop in air (JC-23) that the pour stream remained intact during a 2-m drop with surface tension forcing the leading edge to assume a spherical shape. An exploration was therefore made as to the effect of drag on the spherically shaped leading edge on the pour stream stability.

A calculation is made to determine when drag on an assumed spherically shaped leading edge equals or exceeds the surface tension force necessary to maintain the pour stream continuity. It is assumed that the diameter of the leading edge remains at the orifice diameter, d_o, of 0.025 m. For a first-order approximation, it will be assumed that pour stream velocity will be that for gravitational accelerating, g, in a vacuum

$$u = \frac{dx}{dt} = gt + u_o \tag{D1}$$

$$x = \frac{gt^2}{2} + u_o t \ . \tag{D2}$$

As the stream falls, it accelerates and, therefore, diminishes in diameter, d, according to

$$d = \left[d_o^{\,2} \, u_o/u \right]^{1/2} \ . \tag{D3}$$

The surface tension force, F_s, holding the leading edge to the body of the stream, is

$$F_s = \sigma \pi d \tag{D4}$$

where the surface tension, σ, for Wood's metal is 0.4 N/m.

The drag force, F_d, acting on the leading edge, will be assumed to be the same as for a spherical body with diameter d_o

$$F_d = C_d \frac{\rho u^2}{2} \frac{\pi d_o^2}{4} , \qquad (D5)$$

where C_d, the drag coefficient, is a function of the Reynolds number.[29] The model leads to a Wood's metal breakup length in air or steam of 9.5 m or a L/D_{ji} of 380 (1.2 s after t_o). This model provides an alternative mechanism for pour stream breakup where wave type instabilities of classical theory do not occur in the pour stream as observed in JC-23. It predicts that pour streams about 25 mm in diameter would not break up in a reactor accident scenario until contact with liquid coolant.

The limitations with the above model are:

1. There is no experimental evidence that the leading edge tends to form a sphere with diameter d_o.

2. It does not treat instabilities in an established stream.

3. Both the drag force and surface tension force are acting in the same direction when the pour stream is in a vertical path. Breakup will depend on an instability which will deflect the leading edge in the lateral direction.

4. The theory was simplified in that the effect of drag on the pour stream velocity was not considered.